

Continuum mechanics of entanglement in noisy interacting fermion chains

Tobias Swann¹ and Adam Nahum²

¹*Rudolf Peierls Centre for Theoretical Physics, Clarendon Laboratory, Parks Road, Oxford OX1 3PU, UK*

²*Laboratoire de Physique de l'École Normale Supérieure, CNRS, ENS & Université PSL, Sorbonne Université, Université Paris Cité, 75005 Paris, France*

(Dated: January 30, 2026)

We develop an effective continuum description for information scrambling in a chain of randomly-interacting Majorana fermions. The approach is based on the semiclassical treatment of the path integral for an effective spin chain that describes “two-replica” observables such as the entanglement purity and the OTOC. This formalism gives exact results for the entanglement membrane and for operator spreading in the limit of weak interactions. In this limit there is a large crossover lengthscale between free and interacting behavior, and this large lengthscale allows for a continuum limit and a controlled saddle-point calculation. The formalism is also somewhat different from that known from random unitary circuits. The entanglement membrane emerges as a kind of bound state of two travelling waves, and shows an interesting unbinding phenomenon as the velocity of the entanglement membrane approaches the butterfly velocity.

I. INTRODUCTION

Solvable models for studying chaotic many-body dynamics are rare. Chaotic field theories with a holographic dual provide one solvable regime [1]. Minimal models based on unitary circuits have proven useful for studying entanglement in generic many body systems and have led to putatively universal predictions [2, 3]. By taking noise averages over several replicas of a random unitary circuit, it is possible to express quantities such as the Rényi entanglement entropies as corresponding quantities in a classical statistical mechanics problem. However, random unitary circuits are generally strongly interacting, and the corresponding statistical mechanics problems are discrete problems on the lattice.

Here we consider a different solvable regime, studying a model which is nearly free-fermion but has weak interactions. The consequence of weak interactions is that there is a crossover length scale, beyond which the characteristic interacting behavior emerges, that is much larger than the lattice spacing. As a result we obtain an effective *continuum* model for entanglement, which can be treated in a controlled way using a semiclassical approximation [4].

The weakly interacting fermion model is illuminating for several reasons. First, it confirms the universality of the “entanglement membrane” picture [5–22], for dynamics of quantum information, in a new regime. Second, the present continuum limit gives an alternative source of analytical control. Third, and most interesting, it reveals structures that were not apparent in previous lattice treatments, and which we believe will be relevant to a wider class of models.

For simplicity we focus on an interacting fermion chain with no continuous symmetries (i.e. a Majorana chain) [4], and analyze quantities expressible with $n = 2$ replicas of the circuit and its conjugate: the averages of entanglement purity and of an out-of-time-ordered correlator. The fermion model we study is similar to an SYK chain [23] with noisy couplings [24–27], but our exact results

do not require any “large N ” limit: there is a single Majorana mode on each site. The model can also be viewed as an interacting, Majorana version of the quantum symmetric simple exclusion process [28–30].

The replicated fermion model is mapped to a Heisenberg spin chain that can be treated semiclassically, following [4]. The semiclassical treatment of the path integral for the effective spin chain involves two spacetime fields, $z(x, t)$ and $\bar{z}(x, t)$. By solving their equations of motion, we get a continuum description of the entanglement membrane as a bound state of two smooth domain walls, one in z and one in \bar{z} . We obtain a prediction for the entanglement membrane tension $\mathcal{E}(v)$, which is a function of the velocity v that sets the orientation of the membrane in spacetime, in terms of solutions of differential equations. We discussed the special case of a static membrane, $v = 0$, previously [4]: this case simplifies considerably, because the symmetries of the problem mean that $\bar{z}(x, t) = z(x, t)^*$ and that the solution is time-independent, so that the problem reduces to a simple classical energy minimisation problem for $z(x)$. More generally, it is necessary to address the dynamical problem. Previously the derivation of the entanglement membrane picture has been under quantitative control only in holographic systems (where very complete results, including coupling to hydrodynamics, are available [7, 8]) and in quantum circuits (see e.g. [11, 12, 17, 18]).

In addition to a prediction for $\mathcal{E}(v)$, we also find a qualitative change at a critical velocity v_c where the domain walls in z and \bar{z} become unbound. As $v \rightarrow v_c$ from below, the characteristic size of the bound state diverges like $1/\sqrt{v_c - v}$. In the unbound regime we find two domain walls that travel separately as travelling waves with fixed velocity v_c . This qualitative change at a critical velocity points to ballistic spreading of operators in the Majorana chain, and we identify the critical velocity v_c with the butterfly velocity v_B .

It is interesting to compare the picture we get with the corresponding picture for the Haar-random circuit. There are many similarities, with an emergent entangle-

ment membrane whose effective line tension $\mathcal{E}(v)$ depends on velocity (so that the basic universal features of the dynamics of entanglement and OTOCs agree at the largest lengthscales). However, there are also differences. The effective statistical mechanics model for the circuit can also be formulated in terms of two degrees of freedom which (like z and \bar{z}) are related by time reversal [9], but in the circuit these are summed over separately, whereas z and \bar{z} are not independent in the path integral (even if we allow them to be independent when we search for a saddle point). In the circuit it is convenient to integrate out one of the two degrees of freedom, which simplifies the model at the cost of making time-reversal symmetry no longer manifest. In our continuous model there is not an obvious analog and we treat z and \bar{z} symmetrically.

The present system illustrates how the entanglement structures of the noisy free fermion system (in which, for example, entanglement spreads diffusively) cross over to those of the interacting system. This extends the analysis of our previous paper [4], which considered the crossover due to interactions for the state entanglement after a quench from a product state. A crossover induced by interactions has recently been analyzed [31, 32] in the case of monitored free fermions, using the nonlinear sigma model description [33–36]. However the continuum theory is different in the unitary case and in the monitored case, and the techniques used here will be different.

Travelling wave equations [37, 38] play a role in one part of our the analysis. Various kinds of travelling wave equation have arisen in descriptions of OTOCs [9, 39–47], including in a noisy fermion chain similar to ours but with U(1) charge conservation symmetry [27]. In fact the recent Ref. [48] studies a Majorana chain similar to ours, though with many flavours: while the observables and formalism differ from those here, Ref. [48] arrives at a travelling wave equation equivalent to one that we encounter.

However, the description of the entanglement membrane here involves new ingredients. While the membrane emerges as a solution of the saddle-point equations that propagates at a fixed velocity,¹ this solution is not like a conventional travelling wave, and the saddle-point equations do not in general reduce to conventional travelling wave equations. Instead the entanglement membrane is a “bound state” of waves in two fields, z and \bar{z} , which are related by time-reversal symmetry and for which the natural “arrows of time” are opposite.

II. MODEL

The model we study is a 1D fermionic Hamiltonian with quadratic (free-fermion) nearest-neighbour couplings as well as quartic interactions. For simplicity, both of these are taken to be noisy i.e. varying randomly in both space and time. By a Jordan-Wigner transformation, the model can also be mapped to a generalized Ising model with nearest and next-nearest-neighbour interactions.²

We also assume that the quartic interactions are very weak compared to the free-fermion couplings, as this allows us to derive a continuum model for the spreading of entanglement throughout the chain. If the strength of the quartic interactions were set to exactly zero, then the system would be a free-fermion system, leading to qualitatively different behaviour of the entanglement growth that was discussed in Ref. [4]. However, for any non-zero strength of quartic interactions the system crosses over into the interacting regime at sufficiently long time scales.

We will define our system using a Majorana representation. We take a 1D chain of Majorana modes of length L (with L even). At each site $i = 1, \dots, L$ we have a Majorana operator γ_i , where $\{\gamma_i, \gamma_j\} = 2\delta_{ij}$. The time-dependent Hamiltonian is

$$H_\gamma(t) = -i \sum_i \eta_i(t) \gamma_i \gamma_{i+1} - \sum_i \eta'_i(t) \gamma_i \gamma_{i+1} \gamma_{i+2} \gamma_{i+3}, \quad (1)$$

where $\eta_i(t)$ and $\eta'_i(t)$ are independent Gaussian white noise terms for each i with $\langle \eta_i(t) \eta_j(t') \rangle = \Delta_0^2 \delta_{ij} \delta(t - t')$ and $\langle \eta'_i(t) \eta'_j(t') \rangle = \Delta_I^2 \delta_{ij} \delta(t - t')$. The first term in (1) is a free-fermion term, whereas the second term is an interaction term. Let us define the quantity

$$l_{\text{int}} = \frac{\Delta_0}{\Delta_I}, \quad (2)$$

which we will see later is the appropriate crossover lengthscale. We will consider the limit of weak interactions, so that l_{int} is a large parameter.

In this regime, we find that the parameters Δ_0 and Δ_I in fact drop out of the problem after a rescaling of space and time. That is, the results we obtain for the entanglement line tension are “universal” in the sense that they apply to the model (1) with any choice of Δ_0 and Δ_I , so long as $\Delta_I \ll \Delta_0$ (and in fact for a slightly broader class of lattice models which share the same long-wavelength effective description).

We will calculate how two quantities evolve with time: the entanglement of the time-evolution operator and the

¹ To avoid confusion, we note that we do not use the term “travelling wave” to refer to the bound-state solution, but only to solutions in which only one of z or \bar{z} has nontrivial variation, and for which the equations of motion simplify to FKPP-like equations.

² With noisy terms of the forms X_r and $Z_r Z_{r+1}$ (arising from the free-fermion couplings) and $X_r X_{r+1}$ and $Z_r Z_{r+2}$ (from the fermion interactions), where r is the site index in the Ising chain.

out-of-time-order correlator (OTOC). These can be expressed using tensor products of the time-evolution operator, $U(t) = \mathcal{T} \exp(i \int dt H_\gamma(t))$, and its complex conjugate. In order to fix a concrete basis (and therefore a definite convention for complex conjugation), we may use the Jordan-Wigner mapping of $U(t)$ to the time-evolution operator of a spin-1/2 chain, with $i\gamma_{2r-1}\gamma_{2r} \rightarrow X_r$ and $i\gamma_{2r}\gamma_{2r+1} \rightarrow Z_r Z_{r+1}$ in terms of Pauli matrices. Choosing the Z basis for the qubits, the operators $i\gamma_i\gamma_{i+1}$ correspond to real matrices. Here we will be schematic: see Ref. [4] for more detail.

The entanglement of the time-evolution operator [49–52] is defined by treating the time-evolution operator $\hat{U}(t)$ as a pure state ρ^U in a doubled Hilbert space $\mathcal{H} \otimes \mathcal{H}$ by an operator-to-state mapping. It is then possible calculate the entanglement of this state. In this paper we focus on the average of the entanglement purity

$$e^{-S_2(A)} = \text{Tr}[(\rho_A^U)^2] \quad (3)$$

where ρ_A^U is the reduced density matrix of some subsystem A and we have written the purity in terms of the second Rényi entropy $S_2(A)$. The “subsystem” A can include sites at both the initial time and final time [i.e. both “input” and “output” legs of $\hat{U}(t)$, regarded as a tensor network], because these are considered separate sites after the operator-to-state mapping.

The entanglement of the time-evolution operator is the simplest object that gives access to the entanglement line tension [5]. Choosing subsystem A to include the region to the left of the origin at the initial time, and to the left of point x at the final time, we expect

$$S_2(A) \sim s_{\text{eq}} \mathcal{E}(v) t, \quad (4)$$

where $s_{\text{eq}} = \frac{1}{2} \ln 2$ is the equilibrium entropy density of the physical Majorana chain, in units where the lattice spacing is unity, $v = x/t$, and $\mathcal{E}(v)$ is the “line tension” for the membrane. Above, the constant s_{eq} is factored out for convenience, in order to simplify some identities obeyed by $\mathcal{E}(v)$ [5]. In the present setting it will be useful to further extract a factor of a characteristic velocity v_B , which allows \mathcal{E} to be written in terms of a scaling function g with a dimensionless argument:

$$\mathcal{E}(v) = v_B g\left(\frac{v}{v_B}\right). \quad (5)$$

To be more precise, the line tension we are computing is that associated with the averaged purity: see Refs. [4, 11] for further discussion of this point.

In our explicit treatment, v_B will initially appear as a characteristic velocity $v_c = v_B$ that emerges from the saddle point equations. However, studying the OTOC shows that v_B may be identified with the “butterfly velocity” governing the speed of operator spreading [53–55]. With this identification, the line tension that we compute satisfies conjectured general constraints [5].

The OTOC is defined in terms of the expected absolute square of the commutator of two Heisenberg operators of local observables:

$$\mathcal{C} = \frac{1}{2} \text{Tr} \left[\rho_\infty [\hat{O}_1(0), \hat{O}_2(t)]^\dagger [\hat{O}_1(0), \hat{O}_2(t)] \right] \quad (6)$$

where $\rho_\infty \propto I$ is the infinite temperature thermal density matrix. If $t = 0$ and the operators are spatially separated, they will commute and this quantity will be zero. As t increases, $\hat{O}_2(t)$ will evolve into an increasingly non-local operator with nontrivial support in some increasingly large region. If \hat{O}_1 is outside of this region, the operators will still approximately commute and the above quantity is still approximately zero, but if \hat{O}_1 is inside this region, they fail to commute and the above quantity is positive and of order 1. \mathcal{C} can therefore be used to measure the spreading of an initially local operator under Heisenberg time evolution. Here these operators will be products of Majorana modes.

Each of the above observables can be written as a matrix element of the “replicated” time-evolution operator $U \otimes U^* \otimes U \otimes U^*$; or, after averaging, of

$$\overline{U \otimes U^* \otimes U \otimes U^*} = \exp(-H_{\text{eff}} t). \quad (7)$$

where the overline represents averaging over the white-noise couplings η, η' . Eq. 7 defines the effective Hamiltonian H_{eff} , which acts on a replicated Hilbert space and will be specified explicitly below. Note that formally the right-hand side looks like an “imaginary time” evolution operator, although the physical dynamics is in real time.

We will show that the averaged observables can be approximated by solving coupled classical equations of motion in spacetime which arise from a semiclassical treatment of the path integral for H_{eff} . The two observables (3,6) differ only in the boundary conditions. The resulting classical problem in spacetime involves mobile “domain walls” whose initial and final positions are fixed by these boundary conditions, and the problem reduces to calculating the effective action cost of these domain walls as a function of their velocity.

A. Averaging over disorder

For every different realisation of the random noise $\eta_i(t)$ and $\eta'_i(t)$, the time-evolution operator $U(t)$ will be different, as will the OTOC. Prior to noise-averaging, the replicated time-evolution operator $U \otimes U^* \otimes U \otimes U^*$ describes four replicas for the Majorana chain evolving simultaneously, with the same realisation of the noise:

$$\tilde{H}_\gamma(t) = \sum_{i,a} (-1)^a [i\eta_i(t)\gamma_i^a\gamma_{i+1}^a + \eta'_i(t)\gamma_i^a\gamma_{i+1}^a\gamma_{i+2}^a\gamma_{i+3}^a]. \quad (8)$$

We distinguish the Majorana operators acting on different replicas using the upper index on γ_i^a , with $a = 1, 3$

for the copies that evolve with U , and $a = 2, 4$ for the copies that evolve with U^* . Since we are using a basis where $\gamma_i \gamma_{i+1}$ is purely imaginary, the complex conjugation for the latter leads to the extra minus signs in (8). The noises η and η' are the same for all replicas.

We will discuss boundary conditions in detail later. As a schematic example, the OTOC is a linear function of two copies of the thermal density matrix: after the operator-to-state mapping, the two-copies of the thermal density matrix map to the initial pure state (ket) in the replicated system. The final state (bra) in the replicated system is chosen to yield the desired linear function of the (time-evolved) initial state.

The random variables η and η' are Gaussian so we can explicitly average over noise to get the effective Hamiltonian $H_{\text{eff}} = H_0 + H_I$ where

$$H_0 = -\frac{\Delta_0^2}{2} \sum_i \left[\sum_a (-1)^{a+1} \gamma_i^a \gamma_{i+1}^a \right]^2, \quad (9)$$

$$H_I = -\frac{\Delta_I^2}{2} \sum_i \left[\sum_a (-1)^{a+1} \gamma_i^a \gamma_{i+1}^a \gamma_{i+2}^a \gamma_{i+3}^a \right]^2. \quad (10)$$

As noted above the evolution of the replicated state, using Eq. 7, resembles what is usually called imaginary time evolution.

B. Mapping to spin model

The effective Hamiltonian above has a simple interpretation as the Hamiltonian of a spin chain (cf. Refs. [4, 26, 27, 30, 56, 57]). If we define for each site i the operators

$$A_i^{ab} \equiv -\frac{i}{2} [\gamma_i^a, \gamma_i^b] \quad (11)$$

then the operators $J_i^{ab} \equiv \frac{1}{2} A_i^{ab}$ obey angular momentum commutation relations

$$[J_i^{ab}, J_j^{cd}] = i\delta_{ij}(\delta_{ac}J_i^{bd} + \delta_{bd}J_i^{ac} - \delta_{ad}J_i^{bc} - \delta_{bc}J_i^{ad}) \quad (12)$$

These operators form a representation of the Lie algebra $\text{so}(4)$ at each site i , so we can think of the operators A_i^{ab} as being the equivalents of Pauli matrices acting on an effective “spin” at i . Given that there 4 Majoranas at each site i , the local Hilbert space³ dimension is $2^{4/2} = 4$, and the states in this local Hilbert space transform like spinor representations of $\text{SO}(4)$ [or equivalently as representations of $\text{Spin}(4) \simeq \text{SU}(2) \times \text{SU}(2)$]. This spinor representation is a direct sum of two 2-dimensional irreducible

spinor representations $(1/2, 0)$ and $(0, 1/2)$. The notation indicates that each irreducible representation transforms nontrivially only under one of the two $\text{SU}(2)$ factors of $\text{Spin}(4)$.

Rewriting (9) and (10) using these operators gives

$$H_0 = \Delta_0^2 \sum_i \left[2 - \sum_{a < b} A_i^{ab} A_{i+1}^{ab} \right], \quad (13)$$

$$H_I = \Delta_I^2 \sum_i \left[2 + \sum_{a < b} (-1)^{a+b} A_i^{ab} A_{i+1}^{ab} A_{i+2}^{ab} A_{i+3}^{ab} \right]. \quad (14)$$

The H_0 contribution to the effective spin Hamiltonian is just an $\text{SO}(4)$ -symmetric ferromagnetic Heisenberg interaction, whereas H_I breaks this continuous symmetry down to a discrete symmetry. In the replica formalism, this explicit continuous-symmetry-breaking is the key difference between the interacting and the free system. It changes the structure of the saddle points and also eliminates the gapless Goldstone modes of the replica theory for the noninteracting system.

For our purposes, the model can be simplified: we can define the chirality operator at site i as $\chi_i = -\gamma_i^1 \gamma_i^2 \gamma_i^3 \gamma_i^4$, which has eigenvalues ± 1 , and due to the form of effective Hamiltonian (9) and (10), it follows that each χ_i is individually conserved. The boundary conditions relevant to entanglement and the OTOC impose the values $\chi_i = +1$ for the conserved quantities on all sites, so we can restrict our Hilbert space to just these states. Spins with $\chi_i = +1$ transform as 2-dimensional irreducible representations of one of the $\text{SU}(2)$ subgroups of $\text{Spin}(4)$. Therefore the resulting model is ultimately quite simple, containing only a single $\text{SU}(2)$ spin-1/2 on each site [4, 26, 56], with the Hamiltonian terms

$$H_0 = 2\Delta_0^2 \sum_i [1 - \boldsymbol{\sigma}_i \cdot \boldsymbol{\sigma}_{i+1}] \quad (15)$$

$$H_I = 2\Delta_I^2 \sum_i \left[1 + \sum_{\alpha} (-1)^{\alpha} \sigma_i^{\alpha} \sigma_{i+1}^{\alpha} \sigma_{i+2}^{\alpha} \sigma_{i+3}^{\alpha} \right] \quad (16)$$

where σ_i^{α} is the the α th Pauli for the spin at site i and α is summed over all three Pauli matrices $\alpha = 1, 2, 3$.

In this simplified model, H_0 is an $\text{SO}(3)$ -symmetric *ferromagnetic* Heisenberg interaction, while H_I breaks $\text{SO}(3)$ down to a discrete D_4 symmetry, at the same time opening an energy gap for local excitations above a ground state. The four ground states are uniform product states of either $|\uparrow\rangle, |\downarrow\rangle, |\rightarrow\rangle$ or $|\leftarrow\rangle$.⁴

The problem of computing quantities like entanglement purity or the OTOC as a function of real time t maps to that of calculating transition amplitudes of the

³ As the system is fermionic, the Hilbert space is not strictly a product of local Hilbert spaces, but since the effective model only involves interactions where an even number of Majorana operators act on each site at a time, the dynamics reduces to that of an effective bosonic model.

⁴ $|\uparrow\rangle, |\downarrow\rangle$ denote σ^3 eigenstates and $|\rightarrow\rangle, |\leftarrow\rangle$ denote σ^1 eigenstates. See Sec. VII of [4] for further discussion of symmetries of the effective model.

form $\langle \text{final} | e^{-\hat{H}_{\text{eff}} t} | \text{initial} \rangle$, where $|\text{initial}\rangle$ and $|\text{final}\rangle$ are now states of the SU(2) spin chain (for both the purity of the time evolution operator and the OTOC, these states are in fact product states). In order to calculate such transition amplitudes in the limit of large length and time scales, it will be helpful to use the coherent-state path integral [58, 59].

C. Coherent state path integral

Solving for the full imaginary time evolution of the above spin model is intractable. However, we expect that we can obtain asymptotically exact results from the coherent states path integral [58, 59][4] when t is large and interactions are weak.

Loosely speaking, this is because (i) imaginary-time evolution drives the system towards low-energy-density states at long times, and (ii) the ground states and low-energy excitations of the model simplify in the limit $\Delta_I \rightarrow 0$. In that limit, the model is a Heisenberg ferromagnet, with ground states that are product states of uniformly aligned spins. A standard heuristic statement is that in such low-energy regimes, large blocks of almost-aligned spins act like composite spins with an effective “large S ”, so that semiclassics becomes exact.⁵

We define single-site coherent states as

$$|z_i\rangle = \frac{1}{\sqrt{1+z_i^*z_i}} \begin{pmatrix} 1 \\ z_i \end{pmatrix}, \quad (17)$$

and the coherent states of the entire spin chain can be written as products of these states, $|\{z_i\}\rangle = |z_1\rangle|z_2\rangle\cdots|z_L\rangle$. For what follows we drop indices and write $|z\rangle \equiv |z(x)\rangle$, where the function $z = z(x)$ specifies a product state for the entire chain, in continuum notation.

Taking $\Delta_I \rightarrow 0$ allows us to assume that the spin direction is very slowly varying, and we can take the continuum limit in the coherent state path integral. Transition amplitudes for the chain take the form

$$\langle z_F | e^{-HT} | z_I \rangle = \int_{z(0)=z_I}^{\bar{z}(T)=z_F^*} \mathcal{D}z \exp(-\mathcal{S}). \quad (18)$$

where T is the evolution time, and where the action \mathcal{S} is

$$\mathcal{S} = \int dt H(\bar{z}, z) + \mathcal{S}_{\text{Berry}} + \mathcal{S}_{\text{bdry}}. \quad (19)$$

Here $H(\bar{z}, z) = \langle z | H | z \rangle$ is the “classical” Hamiltonian, and we also get a Berry phase term and a boundary

⁵ See Sec. VD of Ref. [4] (published version) for a slightly more detailed justification of the exactness of semiclassics which extends to the present case (with l_{int} as a large parameter justifying semiclassics). We will not attempt a rigorous justification of the exactness of the method in the limit of small Δ_I/Δ_0 but this would be worthwhile.

term. (We abuse notation slightly by using the symbol H both for the quantum Hamiltonian and the classical Hamiltonian that appears in the action.) The classical Hamiltonian $H = H_0 + H_I$ is given by⁶

$$H_0 = 4\Delta_0^2 \int dx \frac{\bar{z}'z'}{(1+\bar{z}z)^2}, \quad (20)$$

$$H_I = 16\Delta_I^2 \int dx \frac{\bar{z}z(1-\bar{z}^2)(1-z^2)}{(1+\bar{z}z)^4}. \quad (21)$$

The Berry phase contribution is

$$\mathcal{S}_{\text{Berry}} = -\frac{1}{2} \int dx dt \frac{\dot{\bar{z}}z - \bar{z}\dot{z}}{1+\bar{z}z}. \quad (22)$$

In computing a transition amplitude, Eq. 18, using saddle-point, the boundary conditions are as follows. The field z is fixed only at the *initial* boundary, while the field \bar{z} is fixed only at the *final* boundary:

$$z(x, 0) = z_I(x), \quad \bar{z}(x, T) = z_F^*(x). \quad (23)$$

The boundary contribution to the action

$$\mathcal{S}_{\text{bdry}} = -\frac{1}{2} \int dx \ln \frac{(1+z_F^*z(T))(1+\bar{z}(0)z_I)}{(1+z_F^*z_F)(1+z_I^*z_I)} \quad (24)$$

depends on z at the final boundary and \bar{z} at the initial boundary, and is zero when z and \bar{z} agree. (Spatial arguments have been suppressed in the above formulas.)

Varying the action \mathcal{S} with respect to z and \bar{z} gives the coupled equations of motion

$$\dot{z} = -(1+\bar{z}z)^2 \frac{\delta H}{\delta \bar{z}}, \quad (25)$$

$$\dot{\bar{z}} = +(1+\bar{z}z)^2 \frac{\delta H}{\delta z}, \quad (26)$$

where, crucially, z and \bar{z} are treated as independent functions of x and t : at the saddle point, \bar{z} need not be the complex conjugate of z [58, 59][4].

Explicitly, this gives

$$\dot{z} = +4\Delta_0^2 \left(z'' - \frac{2\bar{z}(z')^2}{1+\bar{z}z} \right) - 16\Delta_I^2 \frac{\bar{z}(1-z^2)(1-3\bar{z}^2-3\bar{z}z+\bar{z}^3z)}{(1+\bar{z}z)^3}, \quad (27)$$

$$\dot{\bar{z}} = -4\Delta_0^2 \left(\bar{z}'' - \frac{2z(\bar{z}')^2}{1+\bar{z}z} \right) + 16\Delta_I^2 \frac{\bar{z}(1-\bar{z}^2)(1-3z^2-3\bar{z}z+\bar{z}z^3)}{(1+\bar{z}z)^3}. \quad (28)$$

⁶ In taking the continuum limit, we have assumed that z is slowly varying in x , since for $\Delta_I/\Delta_0 \rightarrow 0$ we expect the gradients to approach zero at sufficiently late times. Indeed taking the leading terms in a gradient expansion gives a self-consistent theory with gradients $\sim \Delta_I/\Delta_0$. For the quadratic term H_0 we take only the lowest term in the gradient expansion (which is quadratic in gradients), and for H_I we take only the zeroth-order term in gradients (i.e. without derivatives) since H_I already has an explicit factor of Δ_I^2/Δ_0^2 relative to H_0 .

By solving these equations of motion and substituting the solutions into the action \mathcal{S} , we can arrive at a saddle-point approximation for the transition amplitude $\langle z_F | e^{-Ht} | z_I \rangle \sim e^{-\mathcal{S}}$.

Given that z and \bar{z} are both real for the boundary conditions we are interested in, it will be convenient to use a slightly different parameterisation for much of what follows, with

$$z = \tan \frac{\theta}{2}, \quad \bar{z} = \tan \frac{\phi}{2}. \quad (29)$$

We will switch between using z and \bar{z} and using θ and ϕ as convenient.

The coupled equations of motion for θ and ϕ are

$$\dot{\theta} = +4\Delta_0^2 \left(\theta'' + (\theta')^2 \tan \frac{\theta - \phi}{2} \right) + \Delta_I^2 F(\theta, \phi), \quad (30)$$

$$\dot{\phi} = -4\Delta_0^2 \left(\phi'' + (\phi')^2 \tan \frac{\phi - \theta}{2} \right) - \Delta_I^2 F(\phi, \theta), \quad (31)$$

where

$$F(\theta, \phi) = 8 \sec^2 \frac{\theta - \phi}{2} \sin 2\theta \left(\tan \frac{\theta - \phi}{2} \sin 2\phi - \cos 2\phi \right). \quad (32)$$

It is important to note that it is possible to set $\Delta_0 = \Delta_I = 1$ in the continuum equations of motion by a rescaling of space and time: there are no dimensionless parameters in this continuum problem. Dimensional analysis shows that the characteristic length and timescales are [4]

$$l \equiv \frac{\Delta_0}{\Delta_I}, \quad \tau \equiv \frac{1}{\Delta_I^2}. \quad (33)$$

Since the Hamiltonian is quadratic in the spatial derivatives, the natural generalization of the model would also be rotationally invariant in dimensions higher than one.

III. CONTINUUM DESCRIPTION OF THE ENTANGLEMENT MEMBRANE

The entanglement purity of the time-evolution operator can be calculated using a saddle-point approximation by choosing appropriate boundary conditions z_I and z_F and then solving for $z(x, t)$ and $\bar{z}(x, t)$. As discussed below, the boundary condition z_I imposes a sharp “domain wall” *initial* condition for z at the spatial origin, and the boundary condition z_F imposes a domain wall *final* condition in \bar{z} at spatial position $X = vT$. In the non-interacting system ($\Delta_I = 0$) these domain walls would spread out essentially diffusively away from the temporal boundaries [4],⁷ but we will see that in the interacting

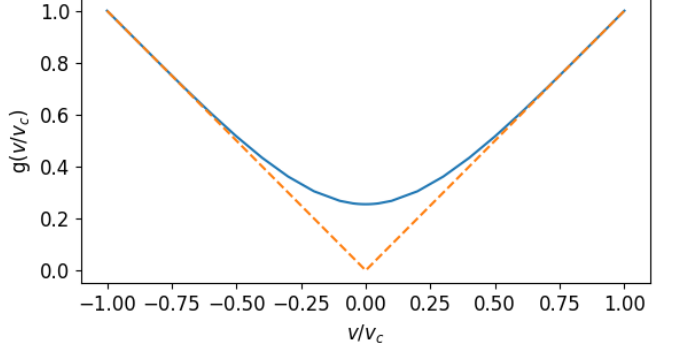


FIG. 1. Plot of $\mathcal{E}(v)$ in terms of the dimensionless function $g(v/v_c)$ in blue, calculated numerically. The dotted orange line shows the asymptote $g_{\text{asymp}}(a) = |a|$ which $g(v/v_c)$ approaches as $v \rightarrow \pm v_c$. (Here $K \equiv \Delta_I/\Delta_0 = 0.005$ was used in the numerics).

system they persist as relatively sharp structures under the effective time evolution.

We will show in Sec. III C that, under certain conditions (for the present observable, this happens if the the velocity v defined by the boundary conditions is not too large) the domain walls in z and \bar{z} form a bound state. By “bound state” we simply mean that they remain close together at all times (i.e. the terminology does not imply that the binding has a simple energetic interpretation). The bound state has an action cost per-unit-time $E(v)$ which is a function of velocity v , and this bound state is the continuum form of the “entanglement membrane” found in other studies of entanglement growth [2, 5–8, 12, 13, 15, 17, 19].

In other conditions (such as sufficiently large v for the present boundary conditions), the domain walls in z and \bar{z} can remain separated by a parametrically large distance, not forming a bound state but instead behaving as independent traveling waves each moving at a fixed velocity. We argue that this velocity is the butterfly velocity v_B and that this is also equal to the maximum velocity v_c at which a domain wall bound state can travel (i.e. $v_c = v_B$). We will discuss this unbound case in Sec. III D.

These two situations are shown schematically in Fig. 2, for the boundary conditions relevant to the time-evolution-operator-entanglement. (This figure only shows the structure on lengthscales of order vT , i.e. it does not resolve the nontrivial structure of the domain walls.) The boundary conditions in the figure will be described below.

One of the main outcomes is the entanglement line tension. We anticipate this result in Fig. 1. The line tension has been written in the form $\mathcal{E}(v) = v_c g(v/v_c)$ (Eq. 5). The function g is then “universal” in the sense that all dependence on the microscopic parameters Δ_0 , $\Delta_I \ll \Delta_0$, and the lattice spacing, has been absorbed into v_c and s_{eq} . Setting the lattice spacing to unity, the

⁷ So that at (for example) $t = T/2$ we would have smooth domain walls with a spatial width of order \sqrt{T} .

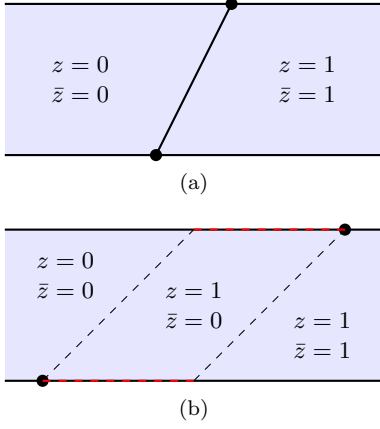


FIG. 2. Schematic of saddle point solution for the time-evolution operator for different values of $|X/T|$, with space plotted horizontally and time vertically. 2(a) shows the solution for $|X/T| < v_c$, with a ballistically travelling bound state connecting the cuts at each boundary (solid line). This is the entanglement membrane. 2(b) shows the solution for $|X/T| > v_c$, with travelling waves propagating from each cut with velocity v_c but remaining isolated from each other (dashed lines). The red dashes show the sections of the boundary which disagree and therefore give an extensive contribution to the boundary action.

critical velocity v_c is

$$v_c = 16\sqrt{2} \Delta_0 \Delta_I, \quad (34)$$

and we will show in Sec. IV that it may also be identified with the butterfly velocity v_B .

Finally, in Sec. III E we will comment on the regime where the speed $|v|$ is very close to, but slightly below, the critical speed v_c . We sketch an analytical argument showing that the spatial extent of the bound state (i.e. of the entanglement membrane) diverges like $1/\sqrt{v_c - |v|}$ as the critical speed is approached, and compare this prediction with numerical results.

A. State entanglement

We first give a brief review of how the replica model can be used to calculate *state* entanglement, following a quench [60] from a weakly-entangled state. We will be schematic, as this observable was covered in detail in [4] for both the free and the interacting case.

In order to calculate the entanglement between a region A of the Majorana chain and its complement \bar{A} , we simply choose appropriate boundary conditions for the coherent state path integral. To find the entanglement of some state of the Majorana chain which has been evolved over a time T , we choose the final state⁸ in the transition amplitude to have all spins pointing right $|\rightarrow\rangle$ within

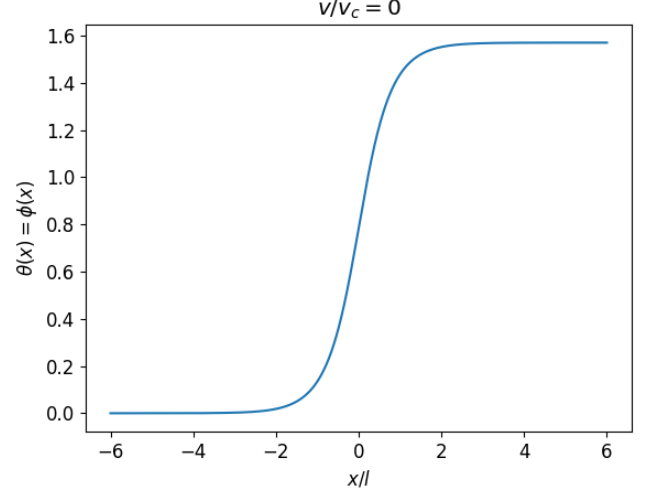


FIG. 3. Static solution of the equations of motion with $\theta(x) = \phi(x)$, determining the rate of growth of state entanglement after a quench from a weakly-entangled state, and the entanglement membrane tension $\mathcal{E}(v)$ at $v = 0$. The exact continuum form of the wall is $\theta(x) = \arctan \exp(2x/l)$ (Eq. 35). This solution is degenerate under spatial translations. Here $l \equiv \Delta_0/\Delta_I$.

the region A and all spins pointing up $|\uparrow\rangle$ outside the region. This fixes the boundary condition for \bar{z} at $t = T$ (compare Eq. 23).

The initial boundary at $t = 0$ is instead determined by the physical initial state of the Majorana chain. After replication, this yields an initial state of the spin chain which is not in fact a coherent state, so slightly more analysis is required. (The cases we address below, which are the focus of this paper, will have simpler, coherent state boundary conditions.) In [4] we argued that generic initial physical states with short-range entanglement enforce a “reflecting” boundary condition $z(x, 0) = \bar{z}(x, 0)$ in the continuum limit.

Let’s take the region A to be the right half of the chain $x > 0$. The boundary conditions at the final time $t = T$ create a domain wall in $\bar{z}(x, T)$, with the $|\uparrow\rangle$ spins in \bar{A} imposing $\bar{z}(x) = 0$ for $x < 0$ and the $|\rightarrow\rangle$ spins in A imposing $\bar{z}(x) = 1$ for $x > 0$.

For $\Delta_I = 0$ the domain wall in $\bar{z}(x)$ relaxes diffusively as time is run “backwards”, away from the final time boundary condition, and in the limit of large the total time T this diffusive spreading allows the domain wall to become arbitrarily wide. But for $\Delta_I > 0$, the domain wall eventually relaxes, after a boundary region of temporal extent $t_{\text{relax}} \sim \Delta_I^{-2}$ near the final-time boundary, to a smooth domain wall with a finite length scale $l_{\text{int}} \sim \Delta_0/\Delta_I$.

We can find the form of this steady state by noticing that (assuming that, for $T \gg t_{\text{relax}}$, a steady state

⁸ In [4], we reversed the time coordinate t so that this boundary

condition was actually applied at $t = 0$ and the physical initial state enforced a boundary condition at $t = T$.

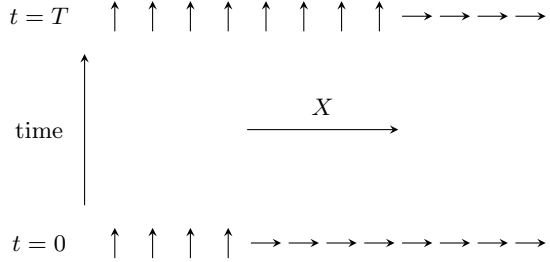


FIG. 4. Initial and final boundary conditions of the spin model used to calculate the entanglement purity of the time-evolution operator. Both boundaries are sharp domain walls with all $|\uparrow\rangle$ to left and $|\rightarrow\rangle$ to the right, with the position of the domain wall translated by X in final boundary compared to the initial one.

is reached in the region away from the final boundary the reflecting boundary condition $z(x, 0) = \bar{z}(x, 0)$ ensures that the steady-state solution satisfies $z(x) = \bar{z}(x)$, or $\theta(x) = \phi(x)$ in the angular parameterisation of Eq. 29. The steady-state property $\dot{z} = \dot{\bar{z}} = 0$ means that the Berry phase term is zero. We can then write the spin Hamiltonian as a function of z alone, and the steady-state solution can then be found by simply minimising the classical energy of $z(x)$ subject the constraints that $z \rightarrow 0$ as $x \rightarrow -\infty$ and $z \rightarrow 1$ as $x \rightarrow +\infty$. This gives (switching to the angular parameterisation for convenience)

$$\theta(x) = \arctan \exp(2x/l), \quad (35)$$

with the length scale $l = \Delta_0/\Delta_I$ as defined in Eq. 33. This solution is shown in Fig. 3. The solution is degenerate under spatial translations, but the symmetry of the boundary conditions ($x \rightarrow -x$ and $\theta \rightarrow \pi/2 - \theta$) implies the above form, with the centre of the smooth domain wall at $x = 0$.

B. Entanglement of the time-evolution operator

When calculating state entanglement, the initial boundary of the spin chain is determined by the physical initial state of the Majorana chain. However, we can also calculate the entanglement of the time evolution operator itself [5, 49–52], by treating both initial and final-time surfaces of the time-evolution operator (viewed as a quantum circuit⁹) as degrees of freedom of a kind of quantum state whose Rényi entanglement entropy can be computed in the usual way. This amounts to performing appropriate contractions for the initial and final-time “legs” (external bonds of the circuit) after replicating the evolution operator.

Take some subset of these legs to be the subsystem A for which we wish to calculate the entanglement purity. In [4], we show that “identity” index contraction taken outside of the subsystem A corresponds to spins in the state $|\uparrow\rangle$, and the “swap” index contraction taken within the subsystem A corresponds to spins in the state $|\rightarrow\rangle$. These boundary states are essentially the states, sometimes denoted $|+\rangle$ and $|-\rangle$, that arise in random circuit calculations from taking traces of powers of the circuit [2].

To study how the time-evolution operator generates entanglement between different parts of the chain, we will take the subsystem A to be $x > 0$ at the initial time $t = 0$ and $x > X$ at the final time $t = T$. This yields a transition amplitude for the spin chain (Eq. 18) in which the initial and the final states each contain a single sharp domain wall, with $|\uparrow\rangle$ to the left of the wall and $|\rightarrow\rangle$ to its right. For $X = 0$ these boundary states are identical, but for $X \neq 0$ the boundary states differ by a spatial translation, as shown in Fig. 4.

The simplest case is for the operator entanglement is $X = 0$, so that both the initial and final boundaries are $|\uparrow\rangle$ for $x < 0$ and $|\rightarrow\rangle$ for $x > 0$. In this case, the problem remains symmetrical under $x \rightarrow -x$ (with $\theta \rightarrow \pi/2 - \theta$ and $\phi \rightarrow \pi/2 - \phi$) and the saddle point solution for θ and ϕ should be roughly constant in time for most of its evolution as long as $T \gg t_{\text{relax}}$. The solution will deviate from this steady state significantly only in boundary regions near $t = 0$ and $t = T$.

The symmetries of the problem mean that we should again expect the steady state to satisfy $z = \bar{z}$, and the solution is simply the same steady state (35) identified for the state entanglement, with the domain wall staying centred at $x = 0$.

C. Moving domain walls and the line tension

We now come to the main focus of this paper, which is saddle point solution when boundary conditions force the domain walls to move. The properties of these moving domain walls tell us directly about the entanglement of the time evolution operator, and we will see in Section IV that they also determine the behaviour of the OTOC.

To do this, we consider the case where the cut in the final boundary is translated by some distance $X > 0$ relative to the cut in the initial boundary. This more general case contains more information about how information spreads spatially over a distance X .

With these boundary conditions, the static domain wall studied in the last section which stays at $x = 0$ would incur an extensive boundary action $\propto X$. However, the fact the static is solution is only unique up to translations suggests that there might also be solutions which drift slowly over time, with an additional action-per-time for these solutions that is quadratic in velocity v for sufficiently small v . Such a drifting domain wall could potentially drift from $x = 0$ at $t = 0$ to $x = X$ at $t = T$, avoiding the boundary cost.

⁹ Here we briefly use a tensor-network language, which we can most simply visualize by e.g. time-discretizing the evolution operator in the Ising representation (Sec. II) to give a quantum circuit.

We therefore look for saddle point solutions which move ballistically at constant velocity v , i.e.

$$\theta(x, t) = \Theta(x - vt) \quad \text{and} \quad \phi(x, t) = \Phi(x - vt). \quad (36)$$

Assuming the solutions have this form, we can convert the problem to a purely spatial one by substituting $\dot{\theta} = -v\theta'$ and $\dot{\phi} = -v\phi'$, so that Eq. (30) becomes

$$\begin{aligned} -v\Theta'(y) = & 4\Delta_0^2 \left(\Theta''(y) + \Theta'(y)^2 \tan \frac{\Theta(y) - \Phi(y)}{2} \right) \\ & + \Delta_I^2 F(\Theta(y), \Phi(y)) \end{aligned} \quad (37)$$

where F was defined in Eq. (32) and

$$y = x - vt \quad (38)$$

is the spatial coordinate in the moving-frame.

Using the symmetry of the problem, we can also assume that

$$\Phi(y) = \pi/2 - \Theta(-y). \quad (39)$$

We can impose this without loss of generality because the solution is defined only up to a translation; the point $y = 0$ is the “centre” of the domain wall by definition.

So finally the saddle-point solution obeys

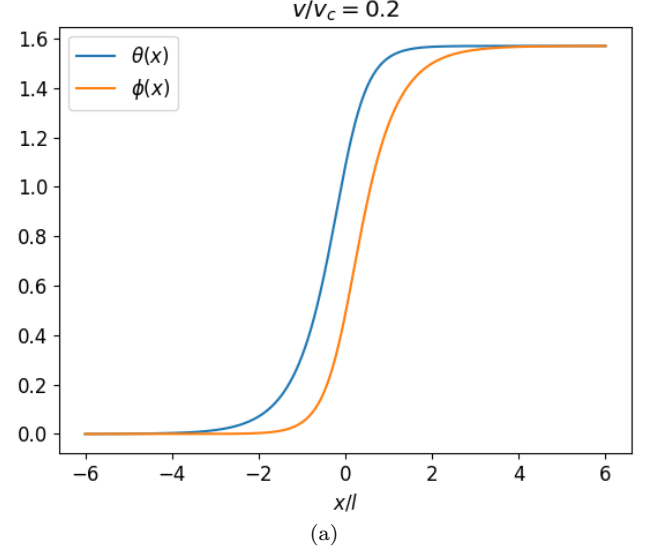
$$\begin{aligned} -v\Theta'(y) = & 4\Delta_0^2 \left(\Theta''(y) + \Theta'(y)^2 \tan \frac{\Theta(y) + \Theta(-y) - \frac{\pi}{2}}{2} \right) \\ & + \Delta_I^2 F(\Theta(y), \pi/2 - \Theta(-y)). \end{aligned} \quad (40)$$

As noted around Eq. 33, the coefficients Δ_0 and Δ_I can be removed from this equation by rescaling both space and time, implying that the solutions have only a trivial dependence on these parameters.

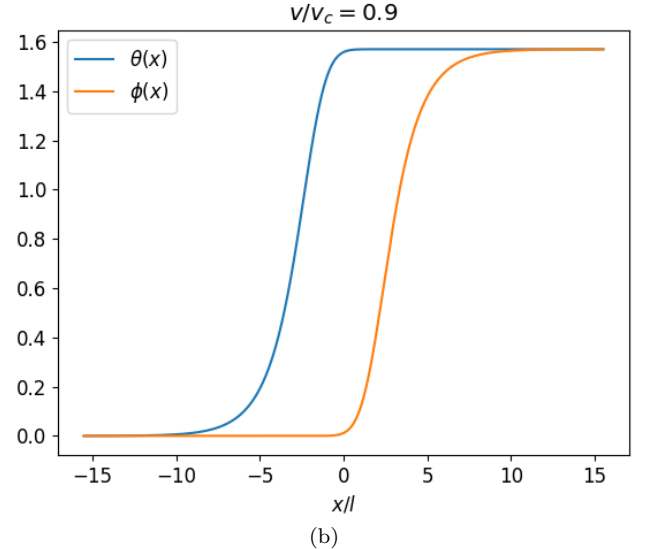
It seems unlikely that the saddle-point equations can be solved analytically in general, but they can be solved numerically using a “fictitious dynamics” that is described in V A. In short, this method uses the equation of motion (30) for $\theta(x, t)$ to evolve θ over time, while continuously keeping $\Phi(y)$ equal to $\pi/2 - \Theta(-y)$ as in Eq. (39). This evolution converges on the desired steady-state solution of Eq. 40. It is important that this method only uses the equation of motion for $\theta(x, t)$ (while continuously enforcing the symmetry which we expect the steady-state solution to have) — this avoids the problem that $\phi(x, t)$ has a negative diffusion coefficient in Eq. 31. The “fictitious dynamics” depends explicitly on v through the symmetry (39) and the fact that $y = x - vt$.

We find numerically that these fictitious dynamics converge to a stable solution whenever the $|v| < v_c$, for the critical velocity v_c which we will discuss in the next section. We show a couple of examples of stable solutions in Fig. 5, illustrating that as v increases, the domain walls in θ and ϕ pull away from each other. (A full discussion of numerical results is deferred until Sec. V.)

Assuming a stable solution can be found for a given v , it is straightforward to numerically calculate the action-per-time using (19). This action has non-zero contributions from both the spin chain Hamiltonian and the Berry



(a)



(b)

FIG. 5. Steady-state solutions of the fictitious dynamics for two velocities in the range $0 < v < v_c$. The domain walls are propagating ballistically to the right with velocity v , with θ “lagging behind” ϕ . Fig. 5(a) shows $v/v_c = 0.2$, where the domain walls in θ and ϕ overlap significantly, while 5(b) shows $v/v_c = 0.9$ where the domain walls propagate almost independently of each other. $x = 0$ is the centre of the domain wall which we use to enforce the symmetry between θ and ϕ (Eq. 39). The length scale l is defined as $l \equiv \Delta_0/\Delta_I$. (Here, $\theta(x)$ $\phi(x)$ were calculated numerically with $K \equiv \Delta_I/\Delta_0 = 0.01$ using the method described in V A).

phase (the Berry phase is actually purely imaginary, and is therefore a real contribution to the action).

If we denote the action per time as a function of v as $E(v)$, we can write the purity of the time-evolution operator as $e^{-E(X/T)T+\dots}$, whenever $|X/T| < v_c$, where the ellipses contain subleading contributions from the regions near the two ends of the domain walls at the temporal boundaries. There is no extensive contribution from the

boundary, since the length scale l on which the domain wall is smoothed is finite, which means that in Eq. (24) $z(T) \approx z_F$ everywhere except within a distance $\sim l$ of the wall.

The dimensional analysis mentioned around Eq. 33 shows that we can extract the constants Δ_0 and Δ_I by writing the cost (action per unit time) of the bound state in terms of a scaling function g as

$$E(v) = s_{\text{eq}} v_c g\left(\frac{v}{v_c}\right) \quad (41)$$

where $s_{\text{eq}} = \frac{1}{2} \ln 2$ is the entropy density, v_c has been defined in Eq. 34, and the function g is “universal”, i.e. independent of Δ_0 and Δ_I . Note that $E(v)$ differs from $\mathcal{E}(v)$ only by the factor of s_{eq} , which is extracted for convenience in defining $\mathcal{E}(v)$.

Our numerical result for the line tension, obtained by the method above, is shown in Fig. 1.

Interestingly the numerical result appears consistent with the conjectured general constraints $\mathcal{E}(v_B) = v_B$, $\mathcal{E}'(v_B) = 1$ [5] if we assume that $v_B = v_c$. In the following Sections we will confirm these identities and show that they arise from nontrivial behaviour of the domain-wall bound state as $|v| \rightarrow v_c$.

D. Travelling waves and determination of v_c

When $|v| > v_c$, the fictitious dynamics do not converge numerically to a steady state solution. Instead, the domain walls in θ and ϕ are widely separated, and the separation grows linearly with time. At late times in this fictitious dynamics, the domain wall in θ is propagating ballistically in a region where $\phi = 0$, but at a speed lower than v , so it cannot “catch up” with the wall in ϕ .

Indeed the true solution for $v > v_c$ involves well-separated domain walls in θ and ϕ . We first study the behaviour of the travelling wave in θ (in a region where $\phi = 0$) on its own.

It is actually more convenient to return to the parameterization using z instead of θ for this problem. The reader is reminded that $z = \tan \frac{\theta}{2}$ and in particular

θ	$-\frac{\pi}{2}$	0	$\frac{\pi}{2}$	π
z	-1	0	1	∞

so the initial boundary conditions are $z = 0$ for $x < 0$ and $z = 1$ for $x > 0$.

The equation we get for z when we set $\bar{z} = 0$ is a travelling wave equation of KPP-Fisher type [37, 38]:

$$\dot{z} = 4\Delta_0^2 z'' - 16\Delta_I^2 z(1 - z^2). \quad (42)$$

After completing this work we learned that this equation has also appeared in recent work on the multi-flavour version of the Majorana chain [48]. The formalism there is somewhat different, but the approach is also based on a semiclassical treatment of the replica theory.

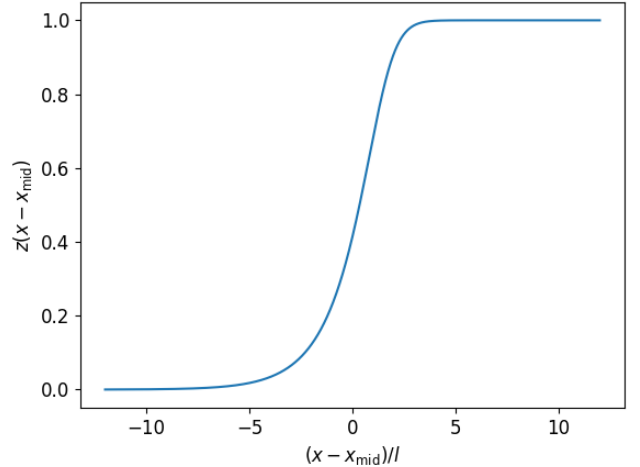


FIG. 6. An example of a right-moving travelling wave solution for z . The midpoint x_{mid} is chosen arbitrarily as the point where $\theta = 2 \arctan z = \pi/4$. (Here, $z(x)$ was found numerically with $K \equiv \Delta_I/\Delta_0 = 0.01$).

This equation admits ballistically travelling solutions at all speeds. However, for a wide range of initial conditions (including the sharp domain wall in our case), the steady state solution travels at a fixed velocity v_* which can be calculated analytically to be

$$v_* = 16\sqrt{2}\Delta_0\Delta_I \quad (43)$$

(see Appendix C for details). This solution is shown in Fig. 6.

Having understood a single domain wall (in z), now let us consider what it tells us about the full problem, with domain walls in both z and \bar{z} . Recall that a velocity $v = X/T$ is defined by the boundary conditions for computing the operator entanglement, and that the “fictitious dynamics”¹⁰ is a method we can use to search for bound-state solutions moving at a given speed v .

First consider the low- v regime. We imagine running the fictitious dynamics with $0 < v < v_*$, and with the domain walls for z and \bar{z} initially well-separated, with the domain wall in z to the left. Then the z -domain wall will move as the travelling wave discussed immediately above, at speed v_* in the rest frame. Such a right-moving travelling wave in z (or θ) will eventually catch up the domain wall in \bar{z} (which is its mirror image in the frame moving at speed v) and collide with it. One may argue that the domain wall in z cannot *overtake* the domain wall in \bar{z} (or a contradiction would result).¹¹ If the domain wall in z cannot lag indefinitely behind the domain wall in \bar{z} ,

¹⁰ See Sec. III C for a brief description of the fictitious dynamics and Sec. V A for more detail.

¹¹ Because then it would enter a region where $\bar{z} \approx 1$, while z still obeys the boundary conditions $z \rightarrow 0$ as $x \rightarrow -\infty$ and $z \rightarrow 1$ as $x \rightarrow +\infty$. Under a change of basis which sends $z = 0$ to $z = 1$ and vice versa, this would again give us Eq. (42), but with

and it also cannot overtake it, the two domain walls must form a bound state travelling with velocity v .

Therefore for $v < v_*$ we indeed expect the fictitious dynamics to converge to a true bound-state solution of the saddle-point equations.

On the other hand if $|v| > v_*$, the domain wall in θ never catches up with its mirror image and travels only as an isolated domain wall, described by (42). Similarly, when we turn from the fictitious dynamics to the true boundary conditions (Sec. III B) then when $v > v_*$ there is a plausible picture [summarized below and in Fig. 2(b) above] with well-separated domain walls in z and \bar{z} that travel along parallel worldlines at speed v_* .

So whenever $|v| < v_*$ we expect a bound state to form, and whenever $|v| > v_*$, we expect no bound state. In other words, we identify v_* with the critical velocity v_c for domain-wall unbinding that was discussed above. This identification fixes the exact value of v_c quoted above in Eq. 34, in agreement with the numerics.

The complete saddle point solution for $|v| > v_c$ has an isolated domain wall in θ travelling from $x = 0$ at $t = 0$ at velocity v_* , reaching the final boundary at $x = v_* T$. Similarly, an isolated domain wall in ϕ starts at $x = X$ at the final time $t = T$ and travels backwards in time at velocity v_* , reaching the initial boundary at $x = X - v_* T$.

As for the bound state regime, we can calculate the action per unit time in the $v > v_c$ regime. Here, the Hamiltonian contribution is zero so the action per time comes entirely from the Berry phase, which we can calculate exactly as $\frac{1}{2} \ln 2 \cdot v_*$ (we get $\frac{1}{4} \ln 2 \cdot v_*$ for each wall). However, unlike for the bound state, there is also a significant boundary contribution, because on each boundary there is a parametrically large gap between the domain walls, where θ and ϕ do not agree. The boundary term gives $\frac{1}{2} \ln 2$ on every site on the boundary for which the two fields do not match, so $\frac{1}{2} \ln 2 \cdot (X - v_* T)$ in total.

The total action is therefore simply $\mathcal{S} = \frac{1}{2} \ln 2 \cdot X$ and the entanglement purity is $\sim e^{-\frac{1}{2} \ln 2 \cdot X}$ for $v > v_c$.

We see that there is a qualitative difference in the entanglement of the time-evolution operator as a function of X and T according to whether we are inside or outside the “light cone” given by $|X/T| = v_c$. This qualitative change is associated with the existence of a bound state of the domain walls in z and \bar{z} only for $v < v_c$.

E. Behaviour of the bound state as $|v| \rightarrow v_c$

We can use the insights of the previous section to investigate the behaviour of the bound state solutions (i.e. the steady-state solutions of Eq. 40 for $|v| < v_c$) as $|v| \rightarrow v_c$ from below. In this limit, the domain walls in θ and ϕ

opposite boundary conditions on z i.e. $z \rightarrow 1$ as $x \rightarrow -\infty$ and $z \rightarrow 0$ as $x \rightarrow +\infty$. This would result in a travelling wave moving to the left with velocity v_* , which is clearly a contradiction.

become further and further apart, and their influence on each other diminishes, and we expect them to increasingly resemble independent travelling waves.

In terms of z and \bar{z} , if \bar{z} really were zero everywhere, then z would be described exactly by Eq. (42), and it would have a travelling wave solution travelling at exactly v_c . The fact that \bar{z} is not exactly zero, and is in fact ≈ 1 in some region sufficiently far in front of the domain wall in z , must lead to the domain wall in z travelling with a lower velocity $v < v_c$.

Ref. [61] analysed the effect of imposing a cutoff of size ε at the front of a travelling wave (a value of the variable below which the exponential growth term is set to zero), and found that this significantly reduces the velocity of the travelling wave, by an amount $\propto 1/(\ln \varepsilon)^2$ at small ε . They also argued that this modification to the velocity was quite robust to the specific way in which the cutoff is implemented. The basic mechanism involves the matching of solutions to the linearized equation for the front in the regions where the cutoff is not active. This approach was later used to study phase transitions in travelling wave problems induced either by a wall moving at an imposed velocity [62] or by a region that the travelling wave is inhibited from entering [63] (related to population growth in a shrinking domain, and to the recursive treatment of tree tensor networks, respectively).

In our case, we do not have a cutoff for $1 - z$ imposed in advance, or a velocity imposed in advance. Nevertheless we expect that a similar mechanism applies. Effectively, in the equation for z we have a position-dependent cutoff that is determined by the form of \bar{z} . From (27), the linearised equation for $\delta z = 1 - z$ reads

$$\delta \dot{z} = 4\Delta_0^2 \delta z'' + 32\Delta_I^2 \left[1 - \frac{6\bar{z}(x)}{(1 + \bar{z}(x))^2} \right] \delta z. \quad (44)$$

In the region where $\bar{z} \approx 0$, we get a travelling wave equation like Eq. (42) which is unstable around $\delta z = 0$, whereas in the region where $\bar{z} \approx 1$, we get a travelling wave equation which is *stable* around $\delta z = 0$. This leads to a more rapid decay of the solution at large x than would be obtained for Eq. (42) and is effectively like a cutoff on the δz equation with ε equal to whatever value δz has at the position of the domain wall in \bar{z} . Matching solutions to the left and the right of this cutoff [61] gives a relation between the velocity and the separation of the domain walls. Of course we could equally well apply the argument to the equation for \bar{z} , instead of that for δz , and we should get a consistent result: here that is guaranteed by symmetry.

Taking the distance between the domain walls in z and \bar{z} to be l_{bs} , the matching argument gives [61]

$$k_{\text{im}} l_{\text{bs}} \sim \frac{\pi}{4} \quad (45)$$

where k_{im} is the imaginary part of the wavenumber k in the solution to the linearised equation $1 - z \propto e^{-k(x-vt)}$, with k_{im} being non-zero for $|v| < v_c$. We can easily calculate $k_{\text{im}} = l^{-1} \sqrt{1 - v/v_c}$ which gives a prediction for

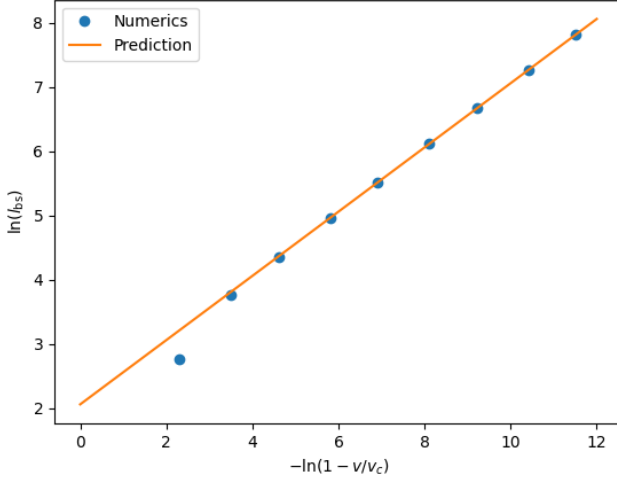


FIG. 7. A log-log plot of the size of the bound state l_{bs} against $1 - v/v_c$ in the limit as $v \rightarrow v_c$, comparing numerical results from the iterative method against the prediction Eq. (46). Given that l_{bs} is only defined up to an additive constant, here the additive constant is chosen to given best agreement with the predicted asymptotic behaviour. (That is, the brown line includes one fitting parameter.) Here $\Delta_I/\Delta_0 = 0.1$.

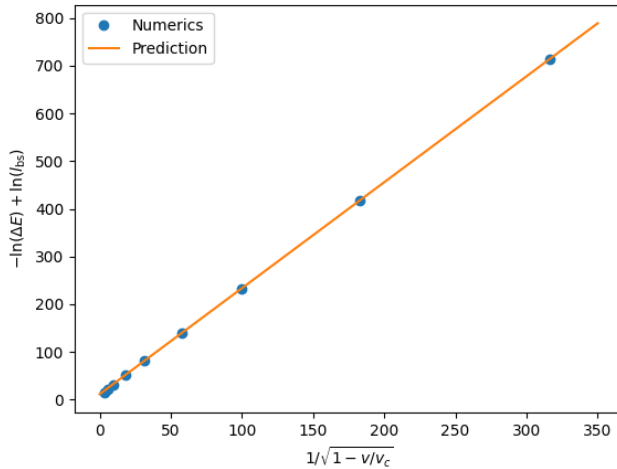


FIG. 8. Numerical test of the prediction in Eq. (47), using the iterative method. We take the log of both sides of the equation and group the $\ln(\Delta E)$ and $\ln(l_{\text{bs}})$ terms together for clarity. In addition to the constant in l_{bs} that was fixed in Fig. 7, the brown line in the present figure includes one new fitting parameter, which is a vertical offset, corresponding to the undetermined overall constant in Eq. 47. In the numerics the parameterisation $1 - z = e^{-h}$ is used to resolve small values of $1 - z$. (Here $\Delta_I/\Delta_0 = 0.1$.)

l_{bs} in the limit $|v| \rightarrow v_c$,

$$l_{\text{bs}} \sim \frac{\pi}{4} \frac{l}{\sqrt{1 - v/v_c}}. \quad (46)$$

This prediction is compared with numerical simulations in Fig. 7. These numerical results are obtained using an iterative procedure, described in Sec. V B, which effi-

ciently finds self-consistent solutions for $|v| \approx v_c$.

We can also use the above approximation to predict the behaviour of the line tension $\mathcal{E}(v)$ as $|v| \rightarrow v_c$. Assuming the fronts of the domain walls resemble the fronts of the travelling waves, and therefore decay exponentially at a rate $k \approx 2\sqrt{2}\Delta_I\Delta_0$ as you move into the interior of the region between the two domain walls, it follows that $\bar{z}(1 - z)$ is of order $e^{-kl_{\text{bs}}}$ in this interior region. Since the nontrivial part of the action is $O(\bar{z}(1 - z))$, a naive guess for the correction to the bound state cost (relative to the cost of independent domain walls in \bar{z} , z) is¹²

$$\Delta E(v) = E(v) - \frac{1}{2} \ln 2 \cdot |v| \propto l_{\text{bs}} \exp\left(-\frac{\pi}{\sqrt{2}} \frac{1}{\sqrt{1 - |v|/v_c}}\right) \quad (47)$$

as $|v| \rightarrow v_c$. This prediction is compared with numerics in Fig. 8.

IV. OUT-OF-TIME-ORDER CORRELATOR

Now we will see how saddle-point solutions closely related to those above can be used to compute the out-of-time-order correlator (OTOC), which is a tool for measuring how Heisenberg operators spread under time evolution [53–55].

Take a local operator \hat{A} supported on some patch near the origin. It commutes with all local operators on sites outside the patch, but not generally with local operators on the same patch. Under Heisenberg time evolution, the operator becomes a linear combination of products of Majoranas with larger and larger support, spreading in all directions. Therefore, the time-evolved operator $\hat{A}(T)$ has a larger commutator with local operators in an ever increasing volume of space. We can quantify this by calculating the expected square of the commutator of the time-evolved operator $\hat{A}(T)$ and a local operator $\hat{B}(0)$ at position X

$$\mathcal{C}(X, T) = \frac{1}{2} \text{Tr} \left[\rho_\infty [\hat{A}(T), \hat{B}(0)]^\dagger [\hat{A}(T), \hat{B}(0)] \right], \quad (48)$$

where ρ_∞ is the infinite temperature density matrix, which is the equilibrium state of the noisy Majorana chain. We will also assume that $\hat{A} = \hat{A}(0)$ and $\hat{B} = \hat{B}(0)$ are bosonic operators, so that they correspond to local observables. This means that they are products of *even* numbers of Majorana operators.

If we take \hat{A} and \hat{B} to be products of Majorana operators (with appropriate factors of i so that they are Hermitian), then $\hat{A}^\dagger = \hat{A}$, $\hat{B}^\dagger = \hat{B}$ and $\hat{A}^2 = \hat{B}^2 = 1$, which gives us the simplified expression

$$\mathcal{C}(X, T) = 1 - \frac{1}{\mathcal{N}} \text{Tr} [\hat{A}(T) \hat{B}(0) \hat{A}(T) \hat{B}(0)] \quad (49)$$

¹² Note that the order of limits we are considering here is $\Delta_I/\Delta_0 \rightarrow 0$ first, and then $v \rightarrow v_c$.

where \mathcal{N} is the dimension of the Hilbert space. The second term in the expression is the OTOC.

If the operator \hat{B} which acts locally at position X is far outside the typical support of the Majorana strings appearing in the expansion of $\hat{A}(T)$, then $\hat{A}(T)$ and \hat{B} essentially commute and the OTOC should be ≈ 1 . However, as the strings appearing in $\hat{A}(T)$ grow to include X , the OTOC should drop to a smaller value (potentially to zero). At any time T , the OTOC should therefore have a lower value within some region, and be ≈ 1 outside this region, with this region growing over time. If this region grows ballistically over time, the velocity with which it grows is called the *butterfly velocity* v_B [9, 39, 53, 54, 64]. This velocity measures the speed at which operators spread out in space under Heisenberg time evolution.

In this Section we first describe how to compute the OTOC and v_B using the coherent-state path integral, and in Sec. IV D we compare with an alternative calculation using an effective Markov process for strings of Majorana modes. This is analogous to the Markov picture for the OTOC in random circuits [9, 64].

We will discuss only the leading-order semiclassical result, which gives v_B in the limit of small Δ_I/Δ_0 . We leave corrections to this semiclassical result (which may be nontrivial), as well as crossovers close to the lightcone, to the future. In the present regime, the Markov picture leads to a particularly simple traveling wave equation.

An interesting range of different travelling wave equations have appeared in studies of the OTOC, including in Fermi liquids [39, 41, 42], long-range-interacting systems [43–45], and quantum circuits in a mean-field-like regime [9, 40] or with weak interactions [46, 47]. In particular, Ref. [26] derived a travelling wave equation, coupled to charge transport, for the OTOC in a noisy fermion chain with U(1) charge conservation symmetry.

A. OTOC boundary conditions

We can use the same approach that we used to calculate the average purity of the time-evolution operator to OTOC in an infinite temperature state (since the noisy chain has no extensive conserved quantities, this is the natural choice of state). To do this, we simply choose the appropriate boundary conditions. Let's say both of the local operators are simply products of neighbouring Majorana operators $\hat{A} = -i\hat{\gamma}_i\hat{\gamma}_{i+1}$ and $\hat{B} = -i\hat{\gamma}_j\hat{\gamma}_{j+1}$. In this case, the initial boundary is all up apart from at i and $i+1$, where the spins are down, $|\cdots\uparrow\uparrow\downarrow\downarrow\uparrow\uparrow\cdots\rangle$, and the final boundary is all right apart from at j and $j+1$ where the spins are left, $|\cdots\rightarrow\rightarrow\leftarrow\leftarrow\rightarrow\rightarrow\cdots\rangle$: see Fig. 9.

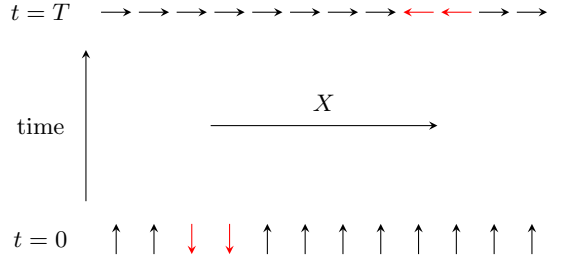


FIG. 9. Initial and final boundary conditions of the spin model used to calculate the averaged OTOC, where both \hat{A} and \hat{B} are of the form $-i\hat{\gamma}_i\hat{\gamma}_{i+1}$. The initial boundary $t = 0$ is $|\uparrow\rangle$ everywhere except where the Majorana operators in \hat{A} act, where it is $|\downarrow\rangle$, and the final boundary $t = T$ is $|\rightarrow\rangle$ everywhere except where the Majorana operators in \hat{B} act, where it is $|\leftarrow\rangle$.

B. Travelling wave solutions for $|X/T| > v_*$

The saddle point solution with the above boundary conditions is a bit less obvious than it was for the entanglement of the time-evolution operator. Let us first consider the simpler case in which X is very large, i.e. $X \gg v_*T$. Let's focus on what happens near the origin. The initial boundary of z is all up except for one spin at the origin which is down. The final boundary is all right. We choose a basis such that right corresponds to $z = 0$ and up corresponds to $z = 1$.

In this basis and in this limit, $\bar{z} = 0$ everywhere near the origin, so we can apply the travelling wave equation (42), which we repeat for convenience:

$$\dot{z} = 4\Delta_0^2 z'' - 16\Delta_I^2 z(1 - z^2). \quad (50)$$

The initial condition for z is $z = 1$ everywhere except at the origin where $z = -1$. With these initial conditions, we get two ballistically propagating travelling waves, one moving in each direction away from the origin. In front of these waves $z = 1$, and in their wake $z = 0$ (not $z = -1$, because this is unstable; the stable state is $z = 0$). Over time, these travelling waves relax to the same travelling wave solutions as before (Sec. III D).

If we assume that this is the solution, and that, by symmetry, the same thing happens in reverse (“backwards in time”) for \bar{z} in the region around $x = X$, then we can calculate the OTOC. We get a contribution from the Berry phase term of $\ln 2v_*T$ and a contribution from the boundary of $-\ln 2v_*T$. These terms cancel out exactly to give $\mathcal{S} = 0$ and the OTOC is 1. This is indeed what we should expect when X is sufficiently large. This solution should hold whenever $|X/T| > v_*$ as $T \rightarrow \infty$, since $|X/T| > v_*$ ensures that the travelling waves in z and \bar{z} remain well-separated.

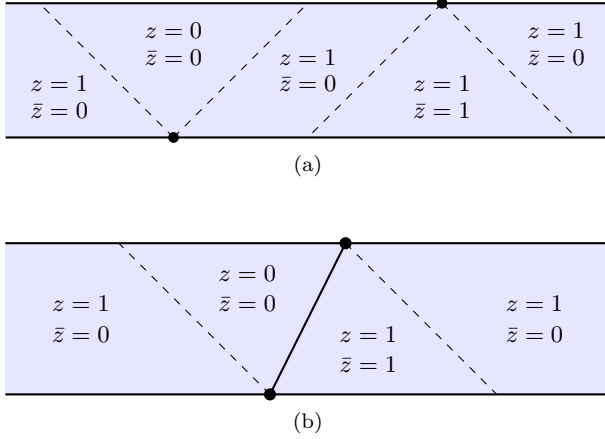


FIG. 10. Schematic of saddle point solution for the OTOC for different values of $|X/T|$. 10(a) shows the solution for $|X/T| > v_c$, where a pair of travelling waves propagate from each boundary point at velocity v_c , without meeting. 10(b) shows the solution for $|X/T| < v_c$, where two of these travelling waves have coalesced into a bound state, while the other two travelling waves are unaffected.

C. Bound state solutions

Let's now consider what happens when $|X/T| < v_*$ with $X > 0$.

If we were to continuously decrease X from above v_*T to below, the right-moving travelling wave in z would collide with the one in \bar{z} . The natural guess is that this reduces the speed of both travelling waves, so that they travel together at speed $v = X/T$, in the bound state solution that we found in the context of the time-evolution operator entanglement: see Fig. 10 (b). The two outer travelling waves, moving in the other direction, are not affected.

The complete solution for $X > 0$ therefore resembles Fig. 10(b), with “outer” traveling waves in z (on the left) and \bar{z} (on the right), and a bound state moving at velocity $v = X/T$ that connects $x = 0, t = 0$ with $x = X, t = T$.

Once again we can calculate the action. We get contributions from the travelling waves, the bound state, and the boundaries. Putting it all together we get a positive action

$$\mathcal{S} = \left(E\left(\frac{X}{T}\right) - \frac{1}{2} \ln 2 \cdot \left| \frac{X}{T} \right| \right) \cdot T, \quad (51)$$

where $E(X/T)T = s_{\text{eq}}\mathcal{E}(X/T)T$ is the nontrivial contribution from the bound state.

This action is proportional to T for any fixed value of value of X/T , and therefore the OTOC is exponentially small, $\sim e^{-\mathcal{S}}$. We see therefore that while the OTOC is 1 outside the light cone $X/T = v_*$, it approaches zero everywhere within this light cone as $T \rightarrow \infty$. We therefore identify the velocity v_* with the butterfly velocity v_B . This identification will be confirmed via the alternative calculation below (Sec. IV D).

By symmetry we obtain an analogous picture for $X < 0$. Interestingly the resulting solution is not smoothly connected to the one we have discussed for $X > 0$. At first sight it is surprising that the saddle point solution shown in Fig. 10(b) should change discontinuously as X changes from positive to negative in order to remain symmetric in X , given that there is no obvious change in the OTOC at this point. However, both saddle point solutions (one with left-moving travelling waves and one with right-moving travelling waves) actually exist for both positive and negative X , although for $X \neq 0$ the contribution of one of these will be exponentially smaller in $|X|$ than the other. This has a close analogue in the random unitary circuit, where the OTOC is related to the probability that the point (X, T) lies in between the endpoints two biased random walks associated with the left and right boundaries of the spreading operator. This can fail to be true either because the right-moving walk ends up to the left of (X, T) , or because the left-moving walk ends up to the right of (X, T) , but for $|X| \gg 1$, one of these possibilities is exponentially less likely than the other.

D. Independent computation of v_B : Effective Markov process

The ballistic spreading of the OTOC can also be understood in terms of a Markov process. Let operator $\hat{A}(t)$ be expressed as sum of products of Majorana operators

$$\hat{A}(t) = \sum_S a_S(t) \hat{\Gamma}_S \quad (52)$$

where S runs over all subsets of sites containing an even number of sites¹³, and $\hat{\Gamma}_S$ is the product over all Majorana operators in S ,

$$\hat{\Gamma}_S = (-i)^{|S|/2} \prod_{i \in S} \hat{\gamma}_i, \quad (53)$$

where the ordering of the product is such that smaller values of i appear to the left of larger values. The operator $\hat{A}(t)$ is then fully described by the real coefficients $a_S(t)$. Note that $\text{Tr}[\hat{\Gamma}_S \hat{\Gamma}_{S'}] = \mathcal{N} \delta_{SS'}$, so $\text{Tr}[\hat{A}(t)^2] = \mathcal{N} \sum_S a_S(t)^2$ is constant over time. If we choose $\hat{A}(0)$ to be a product of Majorana operators then $\sum_S a_S(t)^2 = 1$ at all t .

In Appendix F we show that the noise-averaged values $a_S(t)^2$ obey a master equation corresponding to a

¹³ If we assume that \hat{A} is a bosonic operator which is initially a product of Majorana operators, it must initially be a product of an even number of Majorana operators. Under local time evolution, the operator must remain bosonic, and therefore must be linear combination of products of even numbers of Majorana operators.

fictitious Markov process on subsets of sites (clusters) S ,

$$\frac{d}{dt} \overline{a_S(t)^2} = \sum_{S'} R_{SS'} \overline{a_{S'}(t)^2}, \quad (54)$$

where $\overline{a_S(t)^2}$ is interpreted as the time-dependent probability of configuration S in the fictitious Markov process and $R_{SS'}$ describes the transition rate from configuration S' to configuration S .

The fictitious Markov process involves “particles” at the sites $i \in S$ which hop to unoccupied neighbouring sites at a rate $4\Delta_0^2$; the number of particles can also change when four contiguous sites which contain an odd number of particles all have their occupancies reversed (so one particles becomes three over vice versa) which happens at a rate $4\Delta_I^2$.

The limit $\Delta_I^2 \ll \Delta_0^2$ corresponds to the limit where the particles diffuse for long periods of time and only split or recombine very occasionally. The fact that $\Delta_I^2 \ll \Delta_0^2$ is a continuum limit in the spin model seems to correspond to the fact that, when the particles are sparse, we can think of them as being continuous random walks with diffusion coefficient $4\Delta_0^2$ which only occasionally split into three walks at a rate $4\Delta_I^2$ (and only occasionally recombine).

Define the density of particles ρ_i as the the probability that site i contains a particle, where the probability of a string is $\overline{a_S(t)^2}$: i.e. $\rho_i = \sum_{S|i \in S} \overline{a_S(t)^2}$. If we ignore fluctuations and assume that the particles locally equilibrate much faster than they split or recombine, we can get a continuum equation for the density

$$\frac{\partial \rho}{\partial t} = 4\Delta_0^2 \frac{\partial^2 \rho}{\partial x^2} + 32\Delta_I^2 \rho(1-\rho)(1-2\rho). \quad (55)$$

This is again a Fisher-KPP-like equation: it is actually the same equation as (42) if we make the substitution $\rho = (1-z)/2$. It admits a travelling wave solution with velocity $v_* = 16\sqrt{2}\Delta_0\Delta_I$.

The speed of this travelling wave is the growth rate of the (right-hand boundary of the) operator support, so we again obtain $v_B = v_*$, consistently with the saddle-point approach to the replica spin model.

The Markov mapping in Eq. 54 is exact, while the travelling wave equation (55) arises from a mean-field approximation to this Markov process which we expect to be valid in the limit of small Δ_I/Δ_0 . To go beyond the mean-field approximation we should account for the discreteness of the effective “particles”. Similar effects have been discussed in the context of Brownian quantum circuits in Ref. [40]: a general theory for the effect of discreteness on travelling wave fronts [61, 65] shows that the subleading corrections to v_B are nontrivial and nonanalytic in Δ_I/Δ_0 .

V. NUMERICS

In Sec. III we compared analytical results on the entanglement membrane tension to numerics. We now give

more information on how these simulations were performed.

The equilibrium equation (40) for a domain wall bound state travelling with velocity v is analytically intractable, but can be solved approximately through numerical integration of the “fictitious dynamics” mentioned in Sec. III C. We detail this approach in Sec. V A.

However, as $v \rightarrow v_c$ from below, the fictitious dynamics take arbitrarily long to converge to a steady state solution, so it becomes impractical to study the limiting behaviour of the bound state and $\mathcal{E}(v)$ using this method.

Instead, we use a different iterative method that involves first guessing the form of \bar{z} (which approaches a travelling wave as $v \rightarrow v_c$) and then solving for z by using the known behaviour of $z(x)$ as $x \rightarrow +\infty$. We can then iterate this procedure by using the resulting solution of z to form our new guess for \bar{z} . This procedure converges to a self-consistent solution very quickly when $v \approx v_c$. We discuss this alternative method in Sec V B.

A. Numerically solving the equilibrium equations

How do we find moving bound state solutions for $\theta(x, t)$ and $\phi(x, t)$ in practise? One way is to use the equations of motion.

To motivate the approach, let us first imagine a hypothetical situation where we are *given* the form of ϕ (up to a translation) in the steady state, and only have to determine θ .

As in Eq. 36, we move to the moving frame coordinates (y, t) , writing $\Theta(y, t) = \theta(y + vt, t)$ etc. Then the supplied data is a fixed function $\Phi(y)$ in the moving frame.

Working in this frame, we could evolve $\Theta(y, t)$ forwards in time, starting from an initial state $\Theta(y, 0)$ with a sharp domain wall [$\Theta(y) = 0$ for $x < 0$ and $\Theta(y) = \pi/2$ for $x > 0$], and using the steady-state form for the other field: $\Phi(y, t) = \Phi(y)$. The equation of motion for Θ is “diffusive” in the sense that $\dot{\Theta} \sim +\Theta'' + \dots$, with a positive coefficient for the Θ'' term (contrast the equation for Φ , where this term has the opposite sign). We might therefore expect that as $t \rightarrow \infty$, $\Theta(y, t)$ will approach the desired solution $\Theta(y)$ to the equilibrium equation (37), assuming this solution does exist.

In practice, we do not know the solution for $\Phi(y)$ in advance. We cannot find the equilibrium solution by evolving both $\Theta(y, t)$ and $\Phi(y, t)$ forward in time together, because the equation of motion (31) is $\dot{\Phi} \sim -\Phi'' + \dots$ with a *minus* sign, meaning that Φ only evolves diffusively if we evolve *backwards* in time (evolving forward in time with a generic initial condition will cause small deviations from the equilibrium solution to *grow* exponentially over time).

Fortunately, we do not need to evolve Φ independently from Θ because we already know that reflection symmetry imposes $\Phi(y) = \pi/2 - \Theta(-y)$ (39) in the steady state. Therefore we introduce a fictitious dynamics in which we evolve Θ forwards in time using its equation

of motion, and continuously update Φ so that it satisfies the reflection symmetry of the expected steady state solution. If this dynamics converges to a steady state, then this is automatically a solution of Eq. (40). Explicitly, the fictitious dynamics is

$$\begin{aligned}\dot{\Theta}(y, t) &= v\Theta'(y, t) \\ &+ 4\Delta_0^2 \left(\Theta''(y, t) + \Theta'(y, t)^2 \tan \frac{\Theta(y, t) + \Theta(-y, t) - \frac{\pi}{2}}{2} \right) \\ &+ \Delta_I^2 F(\Theta(y, t), \pi/2 - \Theta(-y, t)),\end{aligned}\quad (56)$$

where the primes are derivatives with respect to y and F is defined in Eq. 32. Since Θ has a positive diffusion coefficient, the dynamics is stable. If Θ approaches a steady state, then this is a saddle-point solution which travels at velocity v .

The way the velocity v enters the problem is in how the “centre” of the domain wall moves (the point around which we reflect θ to get ϕ). This leads to the explicit v -dependence in Eq. (56). Note that we can try to force the centre to move at any given v , but we are not guaranteed a priori that a steady state solution (satisfying the boundary conditions as $y \rightarrow \pm\infty$) will exist for all v .

Numerical integration of Eq. (56) shows that for sufficiently low $|v| < v_c$, with

$$v_c \simeq 22.6 \cdot \Delta_0 \Delta_I \quad (57)$$

there is a stable “bound state” solution, with domain walls in θ and ϕ propagating together, whose action per unit time is a function of v . (The above estimate for v_c is consistent with the analytical result, see Eq. 34 and Sec. IID.) However, for $|v| \geq v_c$, there is no stable solution.

1. Implementation

In order to simulate the fictitious dynamics described above, we first discretise space. In principle, there is a natural discretisation which comes from using the equations of motion for the underlying discrete spin model (15) and (16), but for simplicity we do not use this. Instead, we simply make the substitution $\theta'_i \rightarrow (\theta_{i+1} - \theta_{i-1})/2$ and $\theta''_i \rightarrow \theta_{i+1} + \theta_{i-1} - 2\theta_i$, taking the lattice spacing to be one.

Initially taking $\theta_i = 0$ for $i < 0$ and $\theta_i = \pi/2$ for $i > 0$ (and $\theta_0 = \pi/4$) we update θ_i in each time step according to

$$\begin{aligned}\theta_i &\rightarrow \theta_i + [v\theta'_i + 4\theta''_i + 4(\theta'_i)^2 \tan \frac{\theta_i + \theta_{-i} - \pi/2}{2} \\ &+ K^2 F(\theta_i, \pi/2 - \theta_{-i})]\delta t\end{aligned}\quad (58)$$

where K sets the length scale $l \equiv K^{-1}$. We can think of this as setting $\Delta_0 = 1$ and $\Delta_I = K$, where we take the limit of small K . The parameter δt denotes the size of the small time step taken, but given that we are looking

for steady state solutions where the bracketed term in (58) approaches zero, the results should be insensitive to this parameter, and it is only important that it is small enough for numerics to be stable.

To determine whether or not θ_i has converged, it is important to find a measure of how quickly θ_i is changing which scales appropriately with K (smaller values of $K = l^{-1}$ will lead to smaller derivatives and therefore slower convergence).

Clearly the total change $\sum_i |\dot{\theta}_i|$ will contain a factor of l because the sum will include more sites with large values of $|\dot{\theta}_i|$, so this can be corrected with a factor of $l^{-1} = K$. However, as mentioned above, we also expect smaller values of K to converge over longer time scales. We need to distinguish between the case where $\sum_i |\dot{\theta}_i|$ is small because the solution has converged, and the case where it is small just because the dynamics is slow.

Take two functions, $f_1(t) = ce^{-k_1 t}$ and $f_2(t) = ce^{-k_2 t}$ which agree at $t = 0$ but which decay exponentially at different rates. The condition $f_1(t_1) = f_2(t_2)$ that they both decayed by the same amount translates into the condition on the derivatives $t_1 \dot{f}_1(t_1) = t_2 \dot{f}_2(t_2)$.

We therefore use the following measure for convergence

$$c_K(t) = Kt \sum_i |\dot{\theta}_i(t)| \quad (59)$$

and run the numerics (58) until $c_K(t)$ is decreasing and is below some fixed threshold. For the results in this paper, we used a threshold of 10^{-4} , which gives quantitative results very close to those achieved with smaller thresholds, as long as $|v|/v_c$ is not too close to 1 (for $|v|/v_c$ close to 1 we used a different method described in the following section).

There are two non-trivial checks on the validity of the numerical approach: firstly, when $v = 0$ it should agree with the known analytic solution $\theta(x) = \arctan \exp(2Kx)$; secondly, the numerical value for the velocity v_c above which the bound state gives way to travelling waves should agree with the analytic prediction $v_c = 16\sqrt{2}K$.

Taking $v = 0$, the numeric approximation accurately reproduces the predicted functional and gives the following predicted values for $E(0)$

K	$E(0)$	$E(0)$	ratio
	predicted	numerics	
0.02	0.04	0.03999645...	0.999911...
0.01	0.02	0.01999956...	0.999978...
0.005	0.01	0.00999995...	0.999995...

showing good agreement.

With regards to a qualitative change at $|v| = v_c$, there is clear convergence when v is significantly less than v_c , and clear divergence when v is significantly larger than v_c , but isolating v_c numerically on this basis is difficult because the time taken to converge becomes very large as $v \rightarrow v_c$.

B. Alternative method when $v \approx v_c$

Since the previous method becomes impractical as $|v| \rightarrow v_c$, we study this limit using a completely different method, which converges *faster* for $|v|$ close to v_c .

The basic idea of the alternative method is to make an initial guess $\bar{z}_0(y)$ for $\bar{z}(y)$, and solve the — purely spatial — stationary equation for $z(y)$, obtaining an approximation $z_1(y)$. Using the reflection symmetry, this gives us an improved estimate $\bar{z}_1(y)$ for $\bar{z}(y)$. The process can therefore be iterated to obtain a sequence of estimates $(\bar{z}_k(y), z_k(y))$ which we hope will converge to the true solution.

When $v \lesssim v_c$ this method is effective because we have a good initial estimate $\bar{z}_0(x)$. This initial estimate is given by the free travelling wave solution from Sec. III D. As discussed in Sec. III E, the individual wavefronts making up the bound state are close to the isolated travelling wave form (up to the reflection that relates z and \bar{z}) when $v_c - v$ is small.

In each step we have to solve the spatial equation which has two derivatives and therefore requires two boundary conditions. Fortunately, we can reduce the two unknowns to a single one by solving the equation in the limit $x \rightarrow +\infty$. In this limit, the equation of motion for z can be linearised around $z = 1$, giving the form of z up to a constant factor. This allows us to fix the logarithmic derivative z'/z at the boundary $x \rightarrow +\infty$. This still leaves one unknown e.g. the value of $z(x_0)$ at some point x_0 far to the right, which we deal with using the shooting method.¹⁴

We find that, for $|v|$ sufficiently close to v_c , the solution for z converges after only a few iterations, giving an efficient numerical method to find self-consistent solutions as $v \rightarrow v_c$. We used this method to obtain the data in Figs. 7, 8 above, where we set $\Delta_I/\Delta_0 = 0.1$. For $|v|/v_c \geq 0.9$, the solution essentially converges after a single iteration.

In the limit $|v| \rightarrow v_c$, the forms of domain walls approach those of free travelling waves, meaning that the very first solution we find for z should already be very close to the self-consistent one i.e. even without iterating.

VI. CONCLUSIONS AND OUTLOOK

By mapping the $n = 2$ replica model of the weakly interacting Majorana chain to a spin chain, and rewriting it as a coherent-state path integral, we get a continuum model for operator entanglement which can be solved using a saddle point approximation. The equations of motion involve two fields, $z(x, t)$ and $\bar{z}(x, t)$, or equivalently $\theta(x, t)$ and $\phi(x, t)$, arising initially as parameterisations of spin directions.

If the boundary conditions enforce domain walls, the domain walls in θ and ϕ can form a bound state, which can travel at a range of velocities $|v| < v_c$ for a critical velocity v_c . These bound state solutions acquire an action per time $E(v) = s_{\text{eq}}\mathcal{E}(v)$ and correspond to the entanglement membrane found in previous studies, with $\mathcal{E}(v)$ being the line tension of the membrane for $|v| < v_c$.

If the boundary conditions are such that a bound state would need to travel at $|v| > v_c$, a bound state does not form, and instead the domain walls in θ and ϕ travel independently at the critical velocity v_c , each being described by a Fisher-KPP-like equation. The analysis also shows how the size of the bound state (entanglement membrane) diverges as the critical speed is approached, $l_{\text{bs}} \sim 1/\sqrt{1 - |v|/v_c}$.

The line tension $\mathcal{E}(v)$ and the qualitative change at $|v| = v_c$ allow for predictions about the entanglement of the time-evolution operator and the averaged OTOC. In turn this allows us to identify the critical velocity v_c with the butterfly velocity v_B .

An advantage of the effective continuum model is a weak form of universality of the results: a range of noisy Majorana lattice models, with weak four-fermion interactions, would show the same effective continuum action (19) with some effective parameters Δ_0 and Δ_I . In turn these parameters can be eliminated by rescaling space and time, so that the line tension is governed by a “universal” scaling function $g(v/v_c)$. This means that on large length and time scales, the scrambling properties we have discussed depend only on a length scale $l \equiv \Delta_0/\Delta_I$, a time scale $\tau \equiv \Delta_I^{-2}$ and the equilibrium entropy density s_{eq} .

The length and time scales l and τ mark the crossover between free fermion and interacting behaviour; formally this is due to a crossover from continuous to discrete symmetry [4, 63] which changes the nature of the low-lying excitations of the effective model and its saddle-point solutions.

Now let us mention possible extensions and some questions that we have left open.

First, we have looked here only at two observables, but the coherent-states formalism introduced here and in Ref. [4] could be applied to a much wider range of observables that are expressible using $n \leq 2$ replicas, such as moments of correlation functions [30, 66–72], frame potentials (extending the extensive study in random circuits, see e.g. [73, 74]), or cross-entropies [75, 76].

It would also be interesting to go beyond leading order

¹⁴ We guess $z(x_0)$. If the value we guessed is too high, then when we continue the solution for z to the left using the equation 37, z will diverge in the positive direction. If the value we guessed was too small, it will diverge in the negative direction. As a result, we can always tell whether the value we guessed was too large or too small. Once we have an upper bound z_{max} and lower bound z_{min} on the true value, we can check the middle of this interval $(z_{\text{max}} + z_{\text{min}})/2$ and improve exactly one of these bounds, halving the window. By iterating this procedure, we essentially perform a binary search, finding the true value to arbitrary accuracy in logarithmic time.

in the semiclassical expansion. For example, the Markov process picture can be used to understand subleading corrections to v_B [40, 61] that are nonanalytic in v_I/v_0 , and it would be interesting to see how this effect arises in the path integral approach.

The formalism could also be applied to systems with conserved quantities, as in the noisy QSSEP model [30, 68–72, 77], at the cost of additional fields (compare the monitored systems in [35, 36]), see forthcoming work [78].

For us it was the limit of weak interactions that enabled exact, or numerically exact, results. This limit did not prevent us from studying the genuinely interacting features of quantum chaos: as noted above it simply means that we must examine observables beyond the large crossover scale l in order to see the interacting “universality class”. Similarly, if we move away from the limit of small Δ_I/Δ_0 , we anticipate that the basic bound state picture will remain intact, with the line tension $\mathcal{E}(v)$ receiving additional corrections that are subleading at small Δ_I/Δ_0 and which may be computable by going beyond the leading order in semiclassics.

However, it is not immediately obvious to what extent our results for the regime $v \approx v_c$ are sensitive to the limit of weak interactions that we took (recall that we took this limit prior to approaching v_c). What happens as $v \rightarrow v_c$ at fixed interaction strength? We conjecture that there will still be a diverging bound state size, and an unbound regime for $|v| > v_c$.

For this and for other questions, it may be enlightening to make a more detailed comparison between the random circuit formalism (where at $N = 2$ we usually work with a single “Ising-like” variable, essentially related to z) and the present formalism with two continuum fields that are (loosely speaking) related by time-reversal.

Another open question concerns the fluctuations in (for example) the second Rényi entropy [11]. For the free model, we found numerically in Ref. [4] that fluctuations were sufficiently weak that averaging the purity and averaging the entropy gave the same asymptotic forms at long times: $\overline{S_2} = -\ln e^{-\overline{S_2}} + \text{subleading}$.¹⁵ One might speculate that, here, the two kinds of averages give the same result for $\mathcal{E}(v)$ in the limit of small Δ_I/Δ_0 . One way to approach this is by considering a more general number of replicas and an appropriate limit.

Another challenge that may in principle be addressable in the continuum formalism using the replica trick is to calculate the von Neumann entropy, rather than the second Rényi entropy.

Note added: While we were completing this manuscript we learned of related work by M. Mezei and H. Rajgadlia [79] which also derives the structure

of the entanglement membrane in noisy Majorana chains (Brownian SYK chains). While the approaches used are quite different, the results appear to be consistent where they overlap.

ACKNOWLEDGMENTS

We thank John Chalker, Denis Bernard, Fabian Essler and Andrea De Luca for useful discussion and encouragement and for collaboration on previous related work. We thank the authors of Ref. [79] for correspondence. TS was supported by a James Buckee Scholarship and by Royal Society Enhancement Award (RGF\EA\181042). AN is supported by the European Union (ERC, STAQQ, 101171399). Views and opinions expressed are however those of the authors only and do not necessarily reflect those of the European Union or the European Research Council Executive Agency. Neither the European Union nor the granting authority can be held responsible for them.

Appendix A: Angular parameterisation

The free-fermion Hamiltonian density is

$$h_0 = \Delta_0^2 \sec^2 \frac{\theta - \phi}{2} \theta' \phi' \quad (\text{A1})$$

and the interaction Hamiltonian density is

$$h_I = \Delta_I^2 \sec^4 \frac{\theta - \phi}{2} \sin 2\theta \sin 2\phi \quad (\text{A2})$$

The Berry phase term can be rewritten using

$$\frac{\dot{z}z - \bar{z}\dot{z}}{1 + \bar{z}z} = \frac{\dot{\theta} + \dot{\phi}}{2} \tan \frac{\theta - \phi}{2} - \frac{\dot{\theta}}{2} \tan \frac{\theta}{2} + \frac{\dot{\phi}}{2} \tan \frac{\phi}{2} \quad (\text{A3})$$

$$= \frac{\dot{\theta} + \dot{\phi}}{2} \tan \frac{\theta - \phi}{2} + \frac{\partial}{\partial t} \left[\ln \cos \frac{\theta}{2} - \ln \cos \frac{\phi}{2} \right] \quad (\text{A4})$$

Appendix B: Boundary conditions for the entanglement of the time evolution operator

In order to calculate the entanglement purity of a pure quantum state of the Majorana chain, it is necessary to take a particular “index contraction” of the replicated state, which involves taking the inner product of the states of different replicas which are paired up in a particular way.

For example, the “identity” contraction corresponds to taking the inner product of the state of each ket replica with its corresponding bra replica (so $a = 1$ with $a = 2$ and $a = 3$ with $a = 4$).

Another important index contraction for $N = 2$ is the “swap” contraction, where we take the inner product of

¹⁵ This equality can be checked analytically at very late times, after saturation. In the monitored free Majorana system the equality of the two averages (“annealed” and “quenched”) at leading order follows fairly simply from the structure of saddle points in the replica formalism [34].

the state of each ket replica with *other* bra replica (so $a = 1$ with $a = 4$ and $a = 3$ with $a = 2$).

To calculate the purity of a subsystem A , the identity contraction should be applied outside A to take the partial trace with respect to A and give $\rho_A \otimes \rho_A$, and the swap contraction should be applied within A to give $\text{Tr}[\rho_A^2]$.

In [4] we show that taking the identity contraction at a given spatial site corresponds to contracting with $|\uparrow\rangle$ at the final time, setting a final-time boundary condition at that site, while the swap contraction corresponds to the boundary condition $|\rightarrow\rangle$. Calculating the purity within a region A for a time-evolved pure state $\hat{U}(t)|\psi\rangle$ therefore corresponds to fixing the final state $|\rightarrow\rangle$ within A and $|\uparrow\rangle$ elsewhere.

For this pure state entanglement problem we perform the index contractions only at the final time. However, to calculate the entanglement purity of the time evolution operator $\hat{U}(t)$ itself, we should make the index contractions at both the initial time and final time, so that in the replica model, the replicated initial state $|\psi\rangle \otimes |\psi\rangle^* \otimes |\psi\rangle \otimes |\psi\rangle^*$ of the pure state problem is also replaced by a state corresponding to an index contraction.

Clearly then, in the $SO(3)$ Heisenberg chain, both the initial and final boundary conditions involve contracting with $|\rightarrow\rangle$ within some region A (where A can now include portions of both the initial and final time surfaces) and $|\uparrow\rangle$ outside of A .

Appendix C: Travelling wave review

Eq. 42, which we repeat for convenience,

$$\dot{z} = 4\Delta_0^2 z'' - 16\Delta_I^2 z(1 - z^2), \quad (\text{C1})$$

is a Fisher-KPP type equation [37, 38, 80–83] which can be thought of as the continuum limit of a chain of population growth models with random hoppings between neighbours. Let us briefly review some well-known features.

The equation has two relevant fixed points, a stable one with $z = 0$ everywhere and an unstable one with $z = 1$ everywhere. If initially $0 \leq z(x) \leq 1$ for all x , then this constraint will be true at all times. For generic initial conditions satisfying this constraint, $z(x)$ will at every x eventually approach the stable value $z = 0$, but this will take a long time if x is initially inside a large region with $z = 1$.

Consider the case where $z(x)$ is initially a step function with $z(x) = 0$ for $x < 0$ and $z(x) = 1$ for $x > 0$. Then at late times the solution is a travelling wave, with a $z \sim 0$ region to the left of the wavefront invading a $z \sim 1$ region to its right, at an asymptotically constant velocity $v_* = 16\sqrt{2}\Delta_0\Delta_I$ [37, 38]. In more detail, $z(x - x_t, t)$ converges to the traveling wave solution $f(x)$, where the displacement of the wavefront is $x_t = v_*t + O(\ln t)$ [80, 82].

In the forward tail of the travelling wave, $f = 1 - \Delta f$ with $\Delta f \ll 1$, and one may linearise the equation in Δf [37, 38]. The linearised equation has solutions $\Delta f \sim \exp(-\lambda(x - v(\lambda)t))$ for arbitrary λ , with velocities $v(\lambda) = 4\Delta_0^2\lambda + 32\Delta_I^2/\lambda$. When the initial “domain wall” is sufficiently well-localised, as in the above example, the velocity v_* which emerges at late time is the *minimum* of $v(\lambda)$ over all real λ , occurring for $\lambda_* = 2\sqrt{2}\Delta_I/\Delta_0$. For example, this can be seen by a graphical argument in which we plot $\ln \Delta f$ versus x (see e.g. Ref. [83]). If the initial condition has a right tail that relaxes to $z = 1$ sufficiently slowly as $x \rightarrow +\infty$, then a faster travelling wave can result, but that case is not relevant to our discussion in this paper. See the early parts of Ref. [82] for an overview of the asymptotic behaviour.

Setting $y = x - vt$, the travelling wave solution obeys

$$-vf'(y) = 4\Delta_0^2 f''(y) - 16\Delta_I^2 f(y)(1 - f(y)^2) \quad (\text{C2})$$

with $v = v_*$. This has the form of the equation of motion for a particle moving in one dimension [37, 38]

$$m\ddot{X} = -V'(X) - \gamma\dot{X}, \quad (\text{C3})$$

with mass $m = 4\Delta_0^2$, a potential $V(X) = 4\Delta_I^2(1 - X^2)^2$, and a friction term with coefficient $\gamma = v$. Here $y = x - v_*t$ has been interpreted as a fictitious time coordinate. The boundary conditions are such that the particle is at the local potential maximum $X = 0$ in the distant past ($y \rightarrow -\infty$) and at the potential minimum $X = 1$ in the distant future. The velocity $v = v_*$ is the one for which the motion is critically damped. (For $v < v_*$ the motion would be underdamped, and the particle would oscillate around $X = 1$, which is inconsistent with $z \leq 1$ in the original problem.)

Appendix D: Linear approximation for bound state

When the velocity $v = 0$, the fictitious dynamics settles on a stable domain-wall bound state configuration where $\theta(x) = \phi(x)$. When $v \neq 0$, it is no longer true that $\theta(x) = \phi(x)$, but for small velocities $|v|/v_c \ll 1$ we might expect the difference between θ and ϕ to be small. Here we show that this difference is of order v at small v (so that the separation between the two domain walls is also of order v at small v).

Working with the moving-frame variables Θ and Φ , we can rewrite the equilibrium values in the suggestive form

$$\Theta(x) = \theta_0(x) + \alpha(x) \quad (\text{D1})$$

$$\Phi(x) = \theta_0(x) - \alpha(x) \quad (\text{D2})$$

where α is small when v is small (since the two fields Θ and Φ coincide when $v = 0$). Substituting into the steady state equations for Θ and Φ (see Eq. 40) and expanding in both v and α , we find, at leading nontrivial order,

$$-v\theta'_0 = 4\Delta_0^2\alpha'' + (4\Delta_0^2(\theta'_0)^2 - 8\Delta_I^2(1 + \cos^2 2\theta_0))\alpha, \quad (\text{D3})$$

where θ_0 is the $v = 0$ solution. We see that α is of order v , and we define $\beta(x) \equiv \lim_{v \rightarrow 0} \alpha(x)/(v\Delta_0^{-1}\Delta_I^{-1})$ (recall that $v_c \propto \Delta_0\Delta_I$). For convenience we also set $\Delta_0 = \Delta_I = 1$ by rescaling space and time as discussed in Sec. II C. Finally we substitute in the known analytic solution for θ_0 , to give

$$\beta''(\tilde{x}) = (1 + 3 \tanh^2 2\tilde{x})\beta(\tilde{x}) - \frac{\operatorname{sech} 2\tilde{x}}{4}. \quad (\text{D4})$$

This equation for $\beta(\tilde{x})$ (which can be interpreted as the classical mechanics of a particle in a time-varying force) can be solved numerically with the boundary conditions that $\beta \rightarrow 0$ as $\tilde{x} \rightarrow \pm\infty$.

This solution can then be substituted into the action: this is an independent way to obtain the scaling function $g(v/v_c)$ up to quadratic order in its argument,

$$g(v/v_c) \simeq g(0) + k(v/v_c)^2, \quad (\text{D5})$$

with a numerical value for k which we confirmed was roughly in agreement with the results in the main text.

This approach only gives information for small v , but note that it only involves solving a single equation, rather than a separate equation for each v as in the main text.

Appendix E: Boundary conditions for the OTOC

The OTOC can be written as

$$\frac{1}{\mathcal{N}} \sum_n \langle n | \hat{U}^\dagger(T) \hat{A} \hat{U}(T) \hat{B} \hat{U}^\dagger(T) \hat{A} \hat{U}(T) \hat{B} | n \rangle \quad (\text{E1})$$

where the sum is over some complete basis of states $|n\rangle$.

For each state $|n\rangle$, the operator \hat{B} is applied, then the state is time-evolved forward by T . Then \hat{A} is applied and the state is time-evolved backwards in time by T . This process is repeated and then the final state is contracted with the original state $|n\rangle$. This is then summed for all possible $|n\rangle$.

This can be calculated in the $N = 2$ replica model as follows (assume replicas $a = 1$ and $a = 3$ are “forward” replicas evolving under \hat{U} and replicas $a = 2$ and $a = 4$ and “backward” replicas evolving under \hat{U}^*):

Take the initial state of replica 1 to be $\hat{B}|n\rangle$. This then evolves to $\hat{U}(T)\hat{B}|n\rangle$ at the final time. Then apply \hat{A} at the final time to get $\hat{A}\hat{U}(T)\hat{B}|n\rangle$. Then perform an “identity” index contraction on the final states of replicas 1 and 2 which ensures that the final state of replica 2 is $(\hat{A}\hat{U}(T)\hat{B}|n\rangle)^*$ and therefore the initial state is $(\hat{U}^\dagger(T)\hat{A}\hat{U}(T)\hat{B}|n\rangle)^*$. Applying another index contraction to the initial states of replicas 2 and 3 to ensure that the initial state of replica 3 is $\hat{U}^\dagger(T)\hat{A}\hat{U}(T)\hat{B}|n\rangle$. Repeating this by applying \hat{B} again at the initial time to replica 3, applying \hat{A} at the final time to replica 3 and performing an index contraction to the final states of replicas 3 and 4 similarly ensures that the initial state of replica 4 is $(\hat{U}^\dagger(T)\hat{A}\hat{U}(T)\hat{B}\hat{U}^\dagger(T)\hat{A}\hat{U}(T)\hat{B}|n\rangle)^*$.

Finally, applying and index contraction to the initial states of replicas 1 and 4 gives the sum $\sum_n \langle n | \hat{U}^\dagger(T) \hat{A} \hat{U}(T) \hat{B} \hat{U}^\dagger(T) \hat{A} \hat{U}(T) \hat{B} | n \rangle$, which is simply the OTOC multiplied by the Hilbert space dimension \mathcal{N} .

Therefore the OTOC can be calculated by choosing the following boundary conditions: at the initial time, we pair replica 1 with 4 and pair replica 2 with 3, as well as acting with \hat{B} on replicas 1 and 3. At the final time, we pair replica 1 with 2 and pair replica 3 with 4, as well as acting with \hat{A} on replicas 1 and 3.

The pairing at the initial time is the $N = 2$ “swap” contraction, and corresponds to the state $|\rightarrow\rangle$ in the spin model. However, applying \hat{B} to replicas 1 and 3 swaps the spin direction $|\leftarrow\rangle$ on every site that \hat{B} contains a Majorana operator.

Similarly, the pairing at the final time is the $N = 2$ “identity” contraction, and corresponds to the state $|\uparrow\rangle$ in the spin model. Applying \hat{A} to replicas 1 and 3 swaps the spin direction $|\downarrow\rangle$ on every site that \hat{A} contains a Majorana operator.

Appendix F: Markov process for evolving operator

In order to derive the master equation for the time evolution of $a_S(t)^2$ it will be convenient to Trotterize the time-evolution operator into random unitaries of the form $\exp(\eta\hat{\gamma}_i\hat{\gamma}_{i+1})$ and $\exp(i\eta'\hat{\gamma}_i\hat{\gamma}_{i+1}\hat{\gamma}_{i+2}\hat{\gamma}_{i+3})$, where η and η' are now Gaussian random variables with mean zero and finite variances $\Delta_0^2\delta t$ and $\Delta_I^2\delta t$ respectively. In order to reproduce the continuous time model in the limit $\delta t \rightarrow 0$, in a fixed time interval Δt each type of unitary gate should be applied $\Delta t/\delta t$ times (for each i).

We can now ask how Hermitian operators in the spin chain evolve under the action of these unitary gates. To do this, we only need to know how arbitrary products of Majorana operators evolve, given that any Hermitian operator in the Majorana chain is a linear combination of such products (52). Here we restrict to products of an even number of Majoranas.

For each type of gate we get a discrete Heisenberg equation of motion for the operator \hat{A}

$$\begin{aligned} e^{-\eta\hat{\gamma}_i\hat{\gamma}_{i+1}} \hat{A} e^{\eta\hat{\gamma}_i\hat{\gamma}_{i+1}} &\approx \hat{A} + \eta[\hat{A}, \hat{\gamma}_i\hat{\gamma}_{i+1}] \\ -\eta^2\hat{\gamma}_i\hat{\gamma}_{i+1}\hat{A}\hat{\gamma}_i\hat{\gamma}_{i+1} - \eta^2\hat{A} + O(\eta^3) \end{aligned} \quad (\text{F1})$$

$$\begin{aligned} e^{-i\eta'\hat{\gamma}_i\hat{\gamma}_{i+1}\hat{\gamma}_{i+2}\hat{\gamma}_{i+3}} \hat{A} e^{i\eta'\hat{\gamma}_i\hat{\gamma}_{i+1}\hat{\gamma}_{i+2}\hat{\gamma}_{i+3}} &\approx \hat{A} \\ + i\eta'[\hat{A}, \hat{\gamma}_i\hat{\gamma}_{i+1}\hat{\gamma}_{i+2}\hat{\gamma}_{i+3}] \\ + \eta'^2\hat{\gamma}_i\hat{\gamma}_{i+1}\hat{\gamma}_{i+2}\hat{\gamma}_{i+3}\hat{A}\hat{\gamma}_i\hat{\gamma}_{i+1}\hat{\gamma}_{i+2}\hat{\gamma}_{i+3} \\ - \eta'^2\hat{A} + O(\eta'^3) \end{aligned} \quad (\text{F2})$$

Let's consider the commutators in turn:

If \hat{A} is a product of Majorana operators, then $\hat{\gamma}_i\hat{\gamma}_{i+1}$ commutes with \hat{A} unless \hat{A} contains exactly one of $\hat{\gamma}_i$

or $\hat{\gamma}_{i+1}$. If it does contain exactly one of these, then $[\hat{A}, \hat{\gamma}_i \hat{\gamma}_{i+1}]$ is also proportional to a product of Majorana operators similar to \hat{A} , but $\hat{\gamma}_i$ replaced by $\hat{\gamma}_{i+1}$ or vice versa. This term therefore causes Majorana operators to ‘hop’ to their nearest neighbours. The proportionality factor is $+2$ if $\hat{\gamma}_i$ is replaced by $\hat{\gamma}_{i+1}$, and is -2 if $\hat{\gamma}_{i+1}$ is replaced by $\hat{\gamma}_i$ (the signs won’t be important in the end because the commutator is multiplied by η which has a random sign). So, in the case where \hat{A} does not commute with $\gamma_i \gamma_{i+1}$,

$$e^{-\eta \hat{\gamma}_i \hat{\gamma}_{i+1}} \hat{A} e^{\eta \hat{\gamma}_i \hat{\gamma}_{i+1}} \approx (1 - 2\eta^2) A \pm 2\eta A|_{\gamma_i \leftrightarrow \gamma_{i+1}}. \quad (\text{F3})$$

Similarly, \hat{A} commutes with $\hat{\gamma}_i \hat{\gamma}_{i+1} \hat{\gamma}_{i+2} \hat{\gamma}_{i+3}$ unless \hat{A} contains exactly one or three of the Majorana operators from i to $i+3$. If it doesn’t commute, then $[\hat{A}, \hat{\gamma}_i \hat{\gamma}_{i+1} \hat{\gamma}_{i+2} \hat{\gamma}_{i+3}]$ is a product of Majoranas similar to \hat{A} , but the Majorana operators from i to $i+3$ which did appear \hat{A} no longer appear, and the ones which did not appear in \hat{A} now do appear. This means that either one Majorana operator is replaced by three, or three Majorana operators are replaced by one. Unlike the quadratic terms which simply caused the Majorana operators to hop while conserving their number, the quartic terms allow Majorana operators to be created and destroyed while conserving parity. There is also a factor of ± 2 , with the sign depending on which Majorana operators are replaced. This gives an evolution analogous to (F3).

We can summarise this using the following matrices (recall that S, S' refer to strings of Majorana operators, see Eq. 53)

$$M_{SS'}^{(i)} = \frac{1}{N} \text{Tr} [\hat{\Gamma}_S [\hat{\Gamma}_{S'}, \hat{\gamma}_i \hat{\gamma}_{i+1}]] \quad (\text{F4})$$

$$M'_{SS'}^{(i)} = \frac{1}{N} \text{Tr} [\hat{\Gamma}_S [\hat{\Gamma}_{S'}, \hat{\gamma}_i \hat{\gamma}_{i+1} \hat{\gamma}_{i+2} \hat{\gamma}_{i+3}]] \quad (\text{F5})$$

so $M_{SS'}^{(i)} = 0, \pm 2$ gives the coefficient of $\hat{\Gamma}_S$ coming from the commutator $[\hat{\Gamma}_{S'}, \hat{\gamma}_i \hat{\gamma}_{i+1}]$ and $M'_{SS'}^{(i)}$ does the same for $[\hat{\Gamma}_{S'}, \hat{\gamma}_i \hat{\gamma}_{i+1} \hat{\gamma}_{i+2} \hat{\gamma}_{i+3}]$. Note that, if S can be reached from S' by application of a gate, there is only one possible gate which effects this transition. So if we define

$$M_{SS'} = \sum_i M_{SS'}^{(i)}, \quad (\text{F6})$$

and similarly for M' , then we again have $M_{SS'} = 0, \pm 2$ and $M'_{SS'} = 0, \pm 2$.

Now we assume that, for a particular realisation of the noise η and η' , we know the coefficients $a_S(t)$ in Eq. 52 at some time t . We may define the Trotterization such that, in each δt interval, we apply each kind of unitary gate once for each i . Then we can write the new coefficients

after one more timestep as

$$\begin{aligned} a_S(t + \delta t) \approx & \left(1 - \frac{1}{2} \sum_{S'} M_{S'S}^2 \eta_{S'S}^2 - \frac{1}{2} \sum_{S'} M'_{S'S}^2 \eta'_{S'S}^2 \right) a_S(t) \\ & + \sum_{S'} M_{SS'} \eta_{SS'} a_{S'}(t) + \sum_{S'} M'_{SS'} \eta'_{SS'} a_{S'}(t) \end{aligned}$$

where $\eta_{SS'}$ and $\eta'_{SS'}$ denote the noise terms which multiply the commutators which produce $\hat{\Gamma}_S$ from $\hat{\Gamma}_{S'}$, and in the first line we have used the fact that $M_{S'S}$ and $M'_{S'S}$ are ± 2 whenever they are non-zero. There is only at most one way to produce a given $\hat{\Gamma}_S$ from a given $\hat{\Gamma}_{S'}$, so the noise variables $\eta_{SS'}$ and $\eta'_{SS'}$ for the nonvanishing terms are all independent and are simply a relabelling of the η_i and the η'_i .

We can then write the noise-averaged square of $a_S(t + \delta t)$ conditioned on the previous coefficients $a_S(t)$, which just involves averaging over $\eta_{SS'}$ and $\eta'_{SS'}$ which are independent from $a_S(t)$:

$$\begin{aligned} \mathbb{E}(a_S(t + \delta t)^2 | a_S(t)) \approx & \left(1 - \Delta_0^2 \delta t \sum_{S'} M_{S'S}^2 - \Delta_I^2 \delta t \sum_{S'} M'_{S'S}^2 \right) a_S(t)^2 \\ & + \Delta_0^2 \delta t \sum_{S'} M_{SS'}^2 a_{S'}(t)^2 + \Delta_I^2 \delta t \sum_{S'} M'_{SS'}^2 a_{S'}(t)^2 + \dots, \end{aligned} \quad (\text{F7})$$

where the only second order terms that survive the averaging are ones where the same η or η' appears twice.

To get the unconditional expectation value, we integrate with respect to the coefficients $a_S(t)$ weighted by their probability $P(\{a_S(t)\})$ to get

$$\begin{aligned} \overline{a_S(t + \delta t)^2} \approx & \left(1 - \Delta_0^2 \delta t \sum_{S'} M_{S'S}^2 - \Delta_I^2 \delta t \sum_{S'} M'_{S'S}^2 \right) \overline{a_S(t)^2} \\ & + \Delta_0^2 \delta t \sum_{S'} M_{SS'}^2 \overline{a_{S'}(t)^2} + \Delta_I^2 \delta t \sum_{S'} M'_{SS'}^2 \overline{a_{S'}(t)^2} + \dots. \end{aligned} \quad (\text{F8})$$

or more concisely

$$\overline{a_S(t + \delta t)^2} \approx \overline{a_S(t)^2} + \delta t \sum_{S'} R_{SS'} \overline{a_{S'}(t)^2} \quad (\text{F9})$$

where we have defined

$$R_{SS'} = \Delta_0^2 M_{SS'}^2 + \Delta_I^2 M'_{SS'}^2 \quad (\text{F10})$$

$$- \delta_{SS'} \sum_{S''} (\Delta_0^2 M_{S''S'}^2 + \Delta_I^2 M'_{S''S'}^2). \quad (\text{F11})$$

We can view R as the transition matrix for a stochastic particle hopping problem, with occupied sites corresponding to the sites represented in the string S . $R_{SS'}$

is equal to $4\Delta_0^2$ whenever S and S' differ only by a single particle hopping to an unoccupied nearest neighbour,

and is equal to $4\Delta_I^2$ when S and S' differ only by reversing the occupancies of a set of four contiguous sites that contains an odd number of particles.

[1] Mike Blake, Yingfei Gu, Sean A Hartnoll, Hong Liu, Andrew Lucas, Krishna Rajagopal, Brian Swingle, and Beni Yoshida, “Snowmass white paper: New ideas for many-body quantum systems from string theory and black holes,” arXiv preprint arXiv:2203.04718 (2022).

[2] Matthew PA Fisher, Vedika Khemani, Adam Nahum, and Sagar Vijay, “Random quantum circuits,” Annual Review of Condensed Matter Physics **14**, 335–379 (2023).

[3] Bruno Bertini, Pieter W Claeys, and Tomaž Prosen, “Exactly solvable many-body dynamics from space-time duality,” arXiv preprint arXiv:2505.11489 (2025).

[4] Tobias Swann, Denis Bernard, and Adam Nahum, “Spacetime picture for entanglement generation in noisy fermion chains,” (2023), arXiv:2302.12212 [cond-mat.stat-mech].

[5] Cheryne Jonay, David A Huse, and Adam Nahum, “Coarse-grained dynamics of operator and state entanglement,” arXiv preprint arXiv:1803.00089 (2018).

[6] Adam Nahum, Jonathan Ruhman, Sagar Vijay, and Jeongwan Haah, “Quantum entanglement growth under random unitary dynamics,” Physical Review X **7**, 031016 (2017).

[7] Márk Mezei, “Membrane theory of entanglement dynamics from holography,” Physical Review D **98**, 106025 (2018).

[8] Márk Mezei and Julio Virrueta, “Exploring the membrane theory of entanglement dynamics,” Journal of High Energy Physics **2020**, 1–35 (2020).

[9] Adam Nahum, Sagar Vijay, and Jeongwan Haah, “Operator spreading in random unitary circuits,” Physical Review X **8** (2018), 10.1103/physrevx.8.021014.

[10] Amos Chan, Andrea De Luca, and J. T. Chalker, “Solution of a minimal model for many-body quantum chaos,” Physical Review X **8** (2018), 10.1103/physrevx.8.041019.

[11] Tianci Zhou and Adam Nahum, “Emergent statistical mechanics of entanglement in random unitary circuits,” Phys. Rev. B **99**, 174205 (2019).

[12] Tianci Zhou and Adam Nahum, “Entanglement membrane in chaotic many-body systems,” Physical Review X **10**, 031066 (2020).

[13] Tibor Rakovszky, CW von Keyserlingk, and Frank Pollmann, “Entanglement growth after inhomogenous quenches,” Physical Review B **100**, 125139 (2019).

[14] Jonah Kudler-Flam, Masahiro Nozaki, Shinsei Ryu, and Mao Tian Tan, “Quantum vs. classical information: operator negativity as a probe of scrambling,” Journal of High Energy Physics **2020**, 1–48 (2020).

[15] Cesar A Agón and Márk Mezei, “Bit threads and the membrane theory of entanglement dynamics,” Journal of High Energy Physics **2021**, 1–32 (2021).

[16] Jonah Kudler-Flam, Masahiro Nozaki, Shinsei Ryu, and Mao Tian Tan, “Entanglement of local operators and the butterfly effect,” Physical Review Research **3**, 033182 (2021).

[17] Michael A Rampp, Suhail A Rather, and Pieter W Claeys, “Entanglement membrane in exactly solvable lattice models,” Physical Review Research **6**, 033271 (2024).

[18] Shreya Vardhan and Sanjay Moudgalya, “Entanglement dynamics from universal low-lying modes,” Physical Review B **113**, 014308 (2026).

[19] Tomas Brauner, Sean A Hartnoll, Pavel Kovtun, Hong Liu, Márk Mezei, Alberto Nicolis, Riccardo Penco, Shuheng Shao, and Dam Thanh Son, “Snowmass white paper: effective field theories for condensed matter systems,” arXiv preprint arXiv:2203.10110 (2022).

[20] Hanzhi Jiang, Márk Mezei, and Julio Virrueta, “The entanglement membrane in 2d cft: reflected entropy, rg flow, and information velocity,” Journal of High Energy Physics **2025**, 1–68 (2025).

[21] Ning Bao and Márk Mezei, “On the entropy cone for large regions at late times,” arXiv preprint arXiv:1811.00019 (2018).

[22] Márk Mezei and Wilke van der Schee, “Black holes often saturate entanglement entropy the fastest,” Physical review letters **124**, 201601 (2020).

[23] Debanjan Chowdhury, Antoine Georges, Olivier Parcollet, and Subir Sachdev, “Sachdev-ye-kitaev models and beyond: Window into non-fermi liquids,” Reviews of Modern Physics **94**, 035004 (2022).

[24] Chunxiao Liu, Pengfei Zhang, and Xiao Chen, “Non-unitary dynamics of sachdev-ye-kitaev chain, scipost phys,” arXiv preprint arXiv:2008.11955 (2021).

[25] Pengfei Zhang, Shao-Kai Jian, Chunxiao Liu, and Xiao Chen, “Emergent replica conformal symmetry in non-hermitian syk _2 chains,” Quantum **5**, 579 (2021).

[26] Lakshya Agarwal and Shenglong Xu, “Emergent symmetry in brownian syk models and charge dependent scrambling,” Journal of High Energy Physics **2022**, 1–57 (2022).

[27] Lakshya Agarwal, Subhayan Sahu, and Shenglong Xu, “Charge transport, information scrambling and quantum operator-coherence in a many-body system with u (1) symmetry,” Journal of High Energy Physics **2023**, 1–33 (2023).

[28] Michel Bauer, Denis Bernard, and Tony Jin, “Stochastic dissipative quantum spin chains (i) : Quantum fluctuating discrete hydrodynamics,” SciPost Physics **3** (2017), 10.21468/scipostphys.3.5.033.

[29] Michel Bauer, Denis Bernard, and Tony Jin, “Equilibrium fluctuations in maximally noisy extended quantum systems,” SciPost Physics **6** (2019), 10.21468/scipostphys.6.4.045.

[30] Denis Bernard, Fabian Essler, Ludwig Hruza, and Marko Medenjak, “Dynamics of fluctuations in quantum simple exclusion processes,” SciPost Physics **12**, 042 (2022).

[31] Igor Pohoiko, Paul Pöpperl, Igor V. Gornyi, and Alexander D. Mirlin, “Measurement-induced transitions for interacting fermions,” Physical Review B **111** (2025), 10.1103/physrevb.111.024204.

[32] Haoyu Guo, Matthew S. Foster, Chao-Ming Jian, and Andreas W. W. Ludwig, “Field theory of monitored interacting fermion dynamics with charge conservation,”

Physical Review B **112** (2025), 10.1103/gdxd-pw8v.

[33] Chao-Ming Jian, Hassan Shapourian, Bela Bauer, and Andreas WW Ludwig, “Measurement-induced entanglement transitions in quantum circuits of non-interacting fermions: Born-rule versus forced measurements,” arXiv preprint arXiv:2302.09094 (2023).

[34] Michele Fava, Lorenzo Piroli, Tobias Swann, Denis Bernard, and Adam Nahum, “Nonlinear sigma models for monitored dynamics of free fermions,” .

[35] Igor Pohoiko, Paul Pöpperl, Igor V Gornyi, and Alexander D Mirlin, “Theory of free fermions under random projective measurements,” Physical Review X **13**, 041046 (2023).

[36] Michele Fava, Lorenzo Piroli, Denis Bernard, and Adam Nahum, “Monitored fermions with conserved u (1) charge,” Physical Review Research **6**, 043246 (2024).

[37] A Kolmogorov, I Petrovskii, and N Piskunov, “A study of the diffusion equation with increase in the amount of substance, and its application to a biological problem. translation from: Bulletin of the moscow state university series a 1: 1-26, 1937,” Selected Works of AN Kolmogorov **1**.

[38] Ronald Aylmer Fisher, “The wave of advance of advantageous genes,” Annals of eugenics **7**, 355–369 (1937).

[39] Igor L Aleiner, Lara Faoro, and Lev B Ioffe, “Microscopic model of quantum butterfly effect: out-of-time-order correlators and traveling combustion waves,” Annals of Physics **375**, 378–406 (2016).

[40] Shenglong Xu and Brian Swingle, “Locality, quantum fluctuations, and scrambling,” Physical Review X **9**, 031048 (2019).

[41] Camille Aron, Éric Brunet, and Aditi Mitra, “Traveling discontinuity at the quantum butterfly front,” SciPost Physics **15**, 042 (2023).

[42] Camille Aron, Éric Brunet, and Aditi Mitra, “Kinetics of information scrambling in correlated metals: Disorder-driven transition from shock wave to fisher or kolmogorov-petrovsky-piskunov dynamics,” Physical Review B **108**, L241106 (2023).

[43] Tianci Zhou, Éric Brunet, and Xiaolin Qi, “Operator spreading, duality, and the noisy long-range fkpp equation,” arXiv preprint arXiv:2505.06353 (2025).

[44] Xiao Chen and Tianci Zhou, “Quantum chaos dynamics in long-range power law interaction systems,” Physical Review B **100**, 064305 (2019).

[45] Tianci Zhou, Andrew Guo, Shenglong Xu, Xiao Chen, and Brian Swingle, “Hydrodynamic theory of scrambling in chaotic long-range interacting systems,” Physical Review B **107**, 014201 (2023).

[46] Anna Keselman, Laimei Nie, and Erez Berg, “Scrambling and lyapunov exponent in unitary networks with tunable interactions,” arXiv preprint arXiv:2009.10104 (2020).

[47] Adam Nahum and Andrea De Luca, “unpublished,” .

[48] Onkar Parrikar, Jatin Narde, Harshit Rajgadia, and Sandip Trivedi, “Entanglement spreading and emergent locality in brownian syk chains,” arXiv preprint arXiv:2508.00060 (2025).

[49] Tomaž Prosen and Iztok Pižorn, “Operator space entanglement entropy in a transverse ising chain,” Physical Review A—Atomic, Molecular, and Optical Physics **76**, 032316 (2007).

[50] Tianci Zhou and David J Luitz, “Operator entanglement entropy of the time evolution operator in chaotic systems,” Physical Review B **95**, 094206 (2017).

[51] Paolo Zanardi, “Entanglement of quantum evolutions,” Physical Review A **63**, 040304 (2001).

[52] J Dubail, “Entanglement scaling of operators: a conformal field theory approach, with a glimpse of simulability of long-time dynamics in 1+ 1d,” Journal of Physics A: Mathematical and Theoretical **50**, 234001 (2017).

[53] Daniel A Roberts, Douglas Stanford, and Leonard Susskind, “Localized shocks,” Journal of High Energy Physics **2015**, 1–27 (2015).

[54] Daniel A Roberts and Brian Swingle, “Lieb-robinson bound and the butterfly effect in quantum field theories,” Physical review letters **117**, 091602 (2016).

[55] Shenglong Xu and Brian Swingle, “Scrambling dynamics and out-of-time-ordered correlators in quantum many-body systems,” PRX quantum **5**, 010201 (2024).

[56] Yimu Bao, Soonwon Choi, and Ehud Altman, “Symmetry enriched phases of quantum circuits,” Annals of Physics **435**, 168618 (2021).

[57] Mariya V Medvedyeva, Fabian HL Essler, and Tomaž Prosen, “Exact bethe ansatz spectrum of a tight-binding chain with dephasing noise,” Physical review letters **117**, 137202 (2016).

[58] Michael Stone, Kee-Su Park, and Anupam Garg, “The semiclassical propagator for spin coherent states,” Journal of Mathematical Physics **41**, 8025–8049 (2000).

[59] Julien Tailleur, Jorge Kurchan, and Vivien Lecomte, “Mapping out-of-equilibrium into equilibrium in one-dimensional transport models,” Journal of Physics A: Mathematical and Theoretical **41**, 505001 (2008).

[60] Pasquale Calabrese and John Cardy, “Entanglement entropy and quantum field theory,” Journal of statistical mechanics: theory and experiment **2004**, P06002 (2004).

[61] Eric Brunet and Bernard Derrida, “Shift in the velocity of a front due to a cutoff,” Phys. Rev. E **56**, 2597–2604 (1997).

[62] Bernard Derrida and Damien Simon, “The survival probability of a branching random walk in presence of an absorbing wall,” Europhysics Letters **78**, 60006 (2007).

[63] Adam Nahum, Sthitadhi Roy, Brian Skinner, and Jonathan Ruhman, “Measurement and entanglement phase transitions in all-to-all quantum circuits, on quantum trees, and in landau-ginsburg theory,” PRX Quantum **2**, 010352 (2021).

[64] C. W. von Keyserlingk, Tibor Rakovszky, Frank Pollmann, and S. L. Sondhi, “Operator hydrodynamics, OTOCs, and entanglement growth in systems without conservation laws,” Physical Review X **8** (2018), 10.1103/physrevx.8.021013.

[65] Éric Brunet and Bernard Derrida, “Effect of microscopic noise on front propagation,” Journal of Statistical Physics **103**, 269–282 (2001).

[66] Adam Nahum, Sthitadhi Roy, Sagar Vijay, and Tianci Zhou, “Real-time correlators in chaotic quantum many-body systems,” Physical Review B **106**, 224310 (2022).

[67] Takato Yoshimura, Samuel J Garratt, and JT Chalker, “Operator dynamics in floquet many-body systems,” Physical Review B **111**, 094316 (2025).

[68] Denis Bernard and Tony Jin, “Open quantum symmetric simple exclusion process,” Physical Review Letters **123**, 080601 (2019).

[69] Denis Bernard and Tony Jin, “Solution to the quan-

tum symmetric simple exclusion process: The continuous case,” Communications in Mathematical Physics **384**, 1141–1185 (2021).

[70] Denis Bernard, “Can the macroscopic fluctuation theory be quantized?” Journal of Physics A: Mathematical and Theoretical **54**, 433001 (2021).

[71] Ludwig Hruza and Tony Jin, “Qssep describes the fluctuations of quantum coherences in the anderson model,” arXiv preprint arXiv:2406.06444 (2024).

[72] Guillaume Barraquand and Denis Bernard, “Introduction to quantum exclusion processes,” arXiv preprint arXiv:2507.01570 (2025).

[73] Nicholas Hunter-Jones, “Unitary designs from statistical mechanics in random quantum circuits,” arXiv preprint arXiv:1905.12053 (2019).

[74] Thomas Schuster, Jonas Haferkamp, and Hsin-Yuan Huang, “Random unitaries in extremely low depth,” Science **389**, 92–96 (2025).

[75] Brayden Ware, Abhinav Deshpande, Dominik Hangleiter, Pradeep Niroula, Bill Fefferman, Alexey V Gorshkov, and Michael J Gullans, “A sharp phase transition in linear cross-entropy benchmarking,” arXiv preprint arXiv:2305.04954 (2023).

[76] Alexis Morvan, B Villalonga, X Mi, S Mandrà, A Bengtsson, PV Klimov, Z Chen, S Hong, C Erickson, IK Drozdov, *et al.*, “Phase transitions in random circuit sampling,” Nature **634**, 328–333 (2024).

[77] Mathias Albert, Denis Bernard, Tony Jin, Stefano Scopa, and Shiyi Wei, “Universal classical and quantum fluctuations in the large deviations of current of noisy quantum systems: The case of qssep and qssip,” arXiv preprint arXiv:2601.16883 (2026).

[78] Stefano Scopa, Friedrich Hübner, and Denis Bernard, “Interacting quantum exclusion processes, in progress,” .

[79] Márk Mezei and Harshit Rajgadia, “Entanglement membrane in the brownian syk chain,” arXiv preprint arXiv:2512.04179 (2025).

[80] Maury Bramson, *Convergence of solutions of the Kolmogorov equation to travelling waves*, Vol. 285 (American Mathematical Soc., 1983).

[81] Bernard Derrida and Herbert Spohn, “Polymers on disordered trees, spin glasses, and traveling waves,” Journal of Statistical Physics **51**, 817–840 (1988).

[82] Éric Brunet and Bernard Derrida, “An exactly solvable travelling wave equation in the fisher–kpp class,” Journal of Statistical Physics **161**, 801–820 (2015).

[83] Stéphane Munier, “Lecture notes on ‘quantum chromodynamics and statistical physics’,” arXiv preprint arXiv:1410.6478 (2014).